Check for updates

Received: 30 April 2024 | Accepted: 15 May 2024

DOI: 10.1002/est2.661

REVIEW

ENERGY STORAGE WILEY

A comprehensive review of the aging mechanism and degradation costs of fresh and second-life batteries based on analytical and deterministic methods

Musa Terkes | **Alpaslan Demirci** | **Erdin Gokalp**

Department of Electrical Engineering, Yildiz Technical University, Istanbul, Turkey

Correspondence
Alpaslan Demirci, Department of Electrical Engineering, Yildiz Technical University, Istanbul, Turkey.
Email: ademirci@yildiz.edu.tr

Abstract

Batteries' aging evolution and degradation functions may vary depending on the application area and various stress factors. Studies on its aging characteristics are ongoing, considering the unpredictable tendency of battery degradation during first and secondary usage periods. Battery degradation directly affects operating costs and prevents many stakeholders from making reliable short- or long-term investment plans. Thus, this review study first introduces the battery models commonly used by researchers and provides an overview of the aging mechanism and estimation methods for health status and remaining capacity. Analytical and deterministic aging/degradation functions/models proposed by the researchers are discussed in detail, and cost equations based on degradation are reviewed. This approach was followed for the fresh and second-life batteries by further investigating the impact of stress factors on the aging process and cost. The details of aging prediction approaches based on traditional methods, machine learning, and artificial intelligence are out of the scope of this review article. Discussing the shortcomings of aging analyses/functions and introducing different perspectives on the degradation characteristics will help researchers and provide a roadmap for many stakeholders.

KEYWORDS

analytical and determinictic function and equations, battery aging and degradation mechanism, battery degradation cost, energy storage, second-life battery

1 | INTRODUCTION

Due to global temperature concerns, nations progressively invest significantly more in renewable energy. Energy storage alternatives are critical for increasing renewable energy potential due to the intermittent nature of their energy production and limitations in feed-in to the grid. Lithium-ion batteries have superior storage performance compared to their peers. They have the advantages of low pollution and self-discharge, high energy density, specific energy, discharge current rate, colombic performance, and no memory effect.[1] Accordingly, carbon-neutral forecasts predict the battery market will grow to 832 billion dollars.[2-5] While battery storage solutions can be used in almost any area, aging is inevitable, mainly due to the load profile. Charge/discharge frequency, cycle depth, temperature, charge/discharge rates (C-rate), and the differences in operating current levels may not guarantee the battery life promised by battery manufacturers. Although battery packs are primarily preferred in stationary energy storage applications, their use, especially in electric vehicles (EVs), is increasing by 3%

 © 2024 John Wiley & Sons Ltd.

yearly.[6] Depending on the user profile, customer satisfaction decreases, and the desired driving performance is not achieved after an estimated 5–10 years of first use in the case of EV batteries. In the case of recycling used second-life batteries (SLB) removed from EVs, only 30%–50% of the investment will be recovered.[7] Therefore, SLBs can be reused in less demanding operations and reduce the effort to collect mineral ore and mineral-rich brine in the production of fresh batteries (FB),[8] excess water consumption during production,[9] and carbon emissions from electricity consumption.[10] SLBs are a high-potential storage alternative that extends batteries' lifetimes and avoids costly and difficult recycling processes. However, like FB, SLBs will eventually age.

This review article first introduces the battery models commonly used in the literature and details the aging mechanism of batteries. While the methods for determining the remaining capacity or analyzing the aging behavior are explained briefly, the main objective is to review the analytical or deterministic functions proposed for battery aging. The additional operational cost functions caused by battery degradation are also detailed, while similar aging and degradation cost functions for SLBs are evaluated toward the end. In general, the role of stress factors affecting aging processes in the functions and the aging mechanism is discussed separately. Shortcomings in the degradation functions proposed by the researchers have also been raised. The organization of the review article is as follows: Section 1 provides a brief introduction, while Section 2 explains battery models and equations. Section 3 discusses the battery aging mechanism, while Section 4 presents the analysis methods for battery aging estimation. Section 5 details the analytical and deterministic functions for battery aging, which is also the main objective of this review article. Sections 6 and 7 deal with the degradation cost functions proposed by researchers for the FB and SLB. Section 8 focuses on the conclusion and discussion of the article.

2 | BATTERY MODELS

The battery equivalent model in Figure 1 is often used in the literature. It represents a battery with a dual parallel and series structure that captures the effects of battery dissipation (R_2 and C_2), charge/discharge energy losses (R_O), load transfer resistance (R_1), and double-layer capacitance (C_1).

The characterization of the equivalent circuit is explained by Equations (1)–(4).[11-13] The experimental data are fitted using a non-linear least squares algorithm, and the equivalent circuit model is appropriately determined. When the model is extended to the coupled

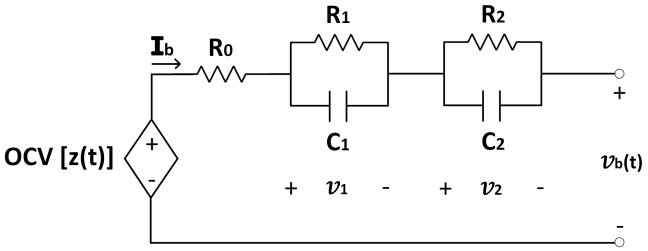


FIGURE 1 Equivalent battery circuit model.[11]

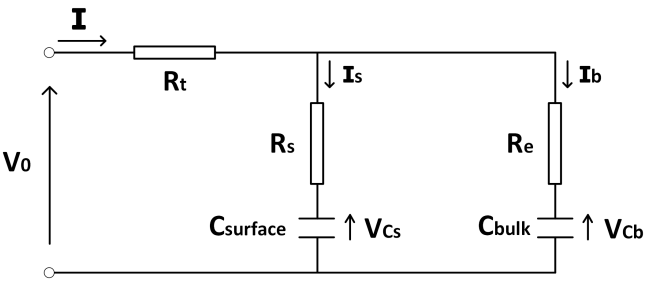


FIGURE 2 RC battery model.[23]

TABLE 1 Li-ion battery initial parameters.[23]

Parameter	Value	Unit
V_{Cb}	883.7283	F
V_{Cs}	82.11	F
R_t	0.002745	Ω
R_e	0.00375	Ω
R_s	0.00375	Ω

electrothermal level, the characterization that considers the battery surface and the internal temperature based on the principle of energy conservation is described by Equations (5) and (6). The equations characterize the Joule heating and heat caused by the entropy change by considering the battery heat conduction resistance (R_C), battery surface (C_S), and internal (C_C) capacity. Half of the sum of $T_C(t)$ and $T_S(t)$ represents the radial mean temperature of the Li-ion battery at time t.[14,15] Other circuit approaches are Randle,[16] dynamic,[17,18] and RC[19-22] battery models. The RC model was used by Babazadeh and Khiabani,[23] which gave successful results for Li-ion and lead-acid. The capacitor represents the battery's surface capacitance and diffusion effects, while the circuit is shown in Figure 2 with terminal, surface, and tip resistance. Using the state vector (x), output vector (y), and input vector (u), the nonlinear formula f(x,u) is obtained as in Equation (7). While its complex formulation can be solved using its equations ($x = [V_{Cb}\, V_{Cs}\, V_o\, \alpha]^T$ and $C(x) = V_o; u = I$) and the initial parameters in Table 1,

25784862, 2024, 4, Downloaded from https://onlinelibrary.wiley.com/doi/10.1002/est2.661 by Yildiz Technical University, Wiley Online Library on [13/06/2024]. See the Terms and Conditions (https://onlinelibrary.wiley.com/terms-and-conditions) on Wiley Online Library for rules of use; OA articles are governed by the applicable Creative Commons License

the major drawback of this model is its inability to model the battery's dynamic behavior. Other drawbacks include neglecting the hysteresis effect, entering the parameter assignment only once, and using the static open circuit voltage (OCV) curve to determine the state of charge (SOC).

$$\frac{di_{R1}}{dt} = -\frac{1}{R_1 C_1} i_{R1}(t) + \frac{1}{R_1 C_1} i_b(t) \tag{1}$$

$$\frac{di_{R2}}{dt} = -\frac{1}{R_2 C_2} i_{R2}(t) + \frac{1}{R_2 C_2} i_b(t) \tag{2}$$

$$\frac{dz(t)}{dt} = z(t_o) - \frac{\eta}{3600.C_N} \int i_b(t) \tag{3}$$

$$v(t) = \mathrm{OCV}(z(t)) - v_1(t) - v_2(t) - R_o i_b(t) \tag{4}$$

$$C_S \frac{dT_S(t)}{dt} = \frac{(T_{\mathrm{amb}} - T_S(t))}{R_u} + \frac{(T_C(t) - T_S(t))}{R_C} \tag{5}$$

$$C_C \frac{dT_C(t)}{dt} = \frac{(T_S(t) - T_C(t))}{R_C} + I(t) T_C(t) \frac{d\mathrm{OCV}(t)}{dT_C(t)} + I(t)(V(t) - \mathrm{OCV}(t)) \tag{6}$$

$$f(x,u) = \left[\frac{R_e}{C_{\mathrm{surf}}(R_e + R_s)^2} - \frac{x_4 R_s}{(R_e + R_s)^2} - \frac{x_4 {R_s}^2}{R_e (R_e + R_s)^2} + \frac{R_s}{C_{\mathrm{surf}}(R_e + R_s)^2} \right] x + \left[\frac{x_4 R_s}{R_e (R_e + R_s)} - \frac{1}{C_{\mathrm{surf}}(R_e + R_s)} \right] x_3 + \left[\frac{R_e^2}{C_{\mathrm{surf}}(R_e + R_s)^2} - \frac{x_4 R_e R_t}{R_e (R_e + R_s)} + \frac{R_t}{C_{\mathrm{surf}}(R_e + R_s)} + \frac{R_e R_s}{C_{\mathrm{surf}}(R_e + R_s)^2} \right] I \tag{7}$$

3 | BATTERY AGING MECHANISM

Figure 3 shows the internal physical and chemical reactions and external properties caused by aging, considering the battery's anode, cathode, and inactive materials. While the internal aging reactions occur at the anode and cathode, the types of reactions and their effects on capacity loss are quite different. While the impact of liquid collectors, binders, and separators on inactive materials is critical, their effect on the electrolyte, anode, and cathode is minor in aging characteristics. In

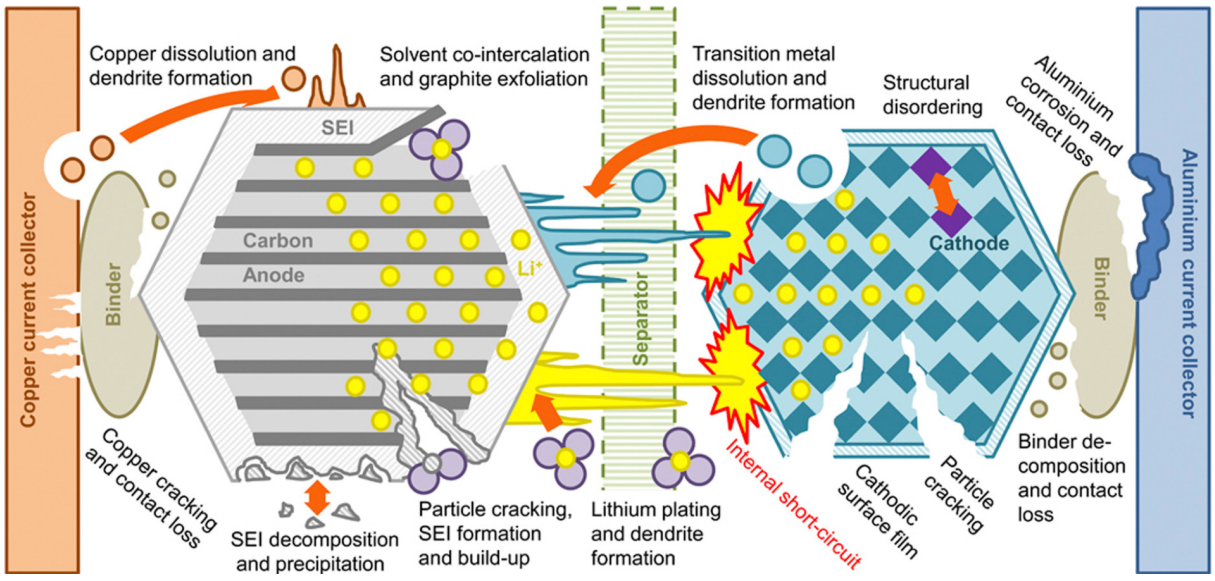


FIGURE 3 Degradation mechanisms in Li-ion cells.[25]

25784862, 2024, 4, Downloaded from https://onlinelibrary.wiley.com/doi/10.1002/est2.661 by Yildiz Technical University, Wiley Online Library on [13/06/2024]. See the Terms and Conditions (https://onlinelibrary.wiley.com/terms-and-conditions) on Wiley Online Library for rules of use; OA articles are governed by the applicable Creative Commons License

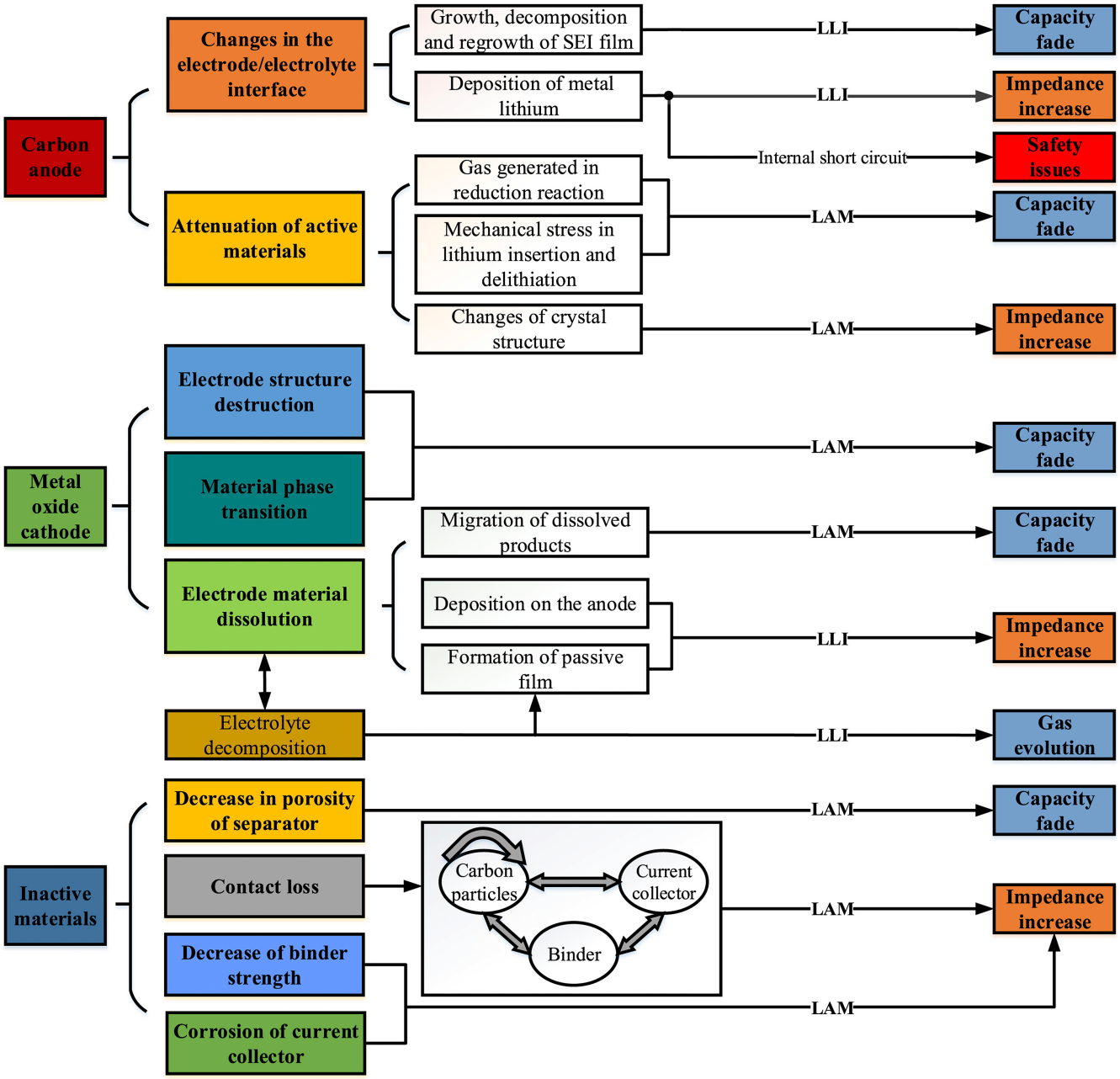


FIGURE 4 Overview of basic physical and chemical reactions inside a battery.[26]

addition, anodic corrosion, loss of active mass, lead sulfate formation, and electrolyte stratification determine the aging behavior of batteries.[24] Besides the electrochemical reaction, loss of lithium-ion inventory (LLI) and loss of active material (LAM) due to side reactions are the main causes of aging. LAM is caused by collector corrosion, binder decomposition, transition metal dissolution, and electrode particle cracking. At the same time, LLI is accelerated by solid electrolyte interfacial film (SEI) rupture and re-formation, electrolyte decomposition, and lithium loss. Due to SEI formation and lithium-ion accumulation on the negative electrode surface, the capacity decreases, and the internal resistance increases. The layer does not ensure lithium ion decomposition and the desired transition but instead consists of side reactions due to lithium-ion consumption. The increase in internal resistance accelerates the upper cut-off limit in terminal voltage, while battery performance gradually degrades with repeated charge-discharge cycles. There are reversible capacity losses due to self-discharge and irreversible capacity losses due to variations in temperature, pre-storage SOC, and storage duration. The aging mechanism can be seen in Figure 4.

25784862, 2024, 4, Downloaded from https://onlinelibrary.wiley.com/doi/10.1002/est2.661 by Yildiz Technical University, Wiley Online Library on [13/06/2024]. See the Terms and Conditions (https://onlinelibrary.wiley.com/terms-and-conditions) on Wiley Online Library for rules of use; OA articles are governed by the applicable Creative Commons License

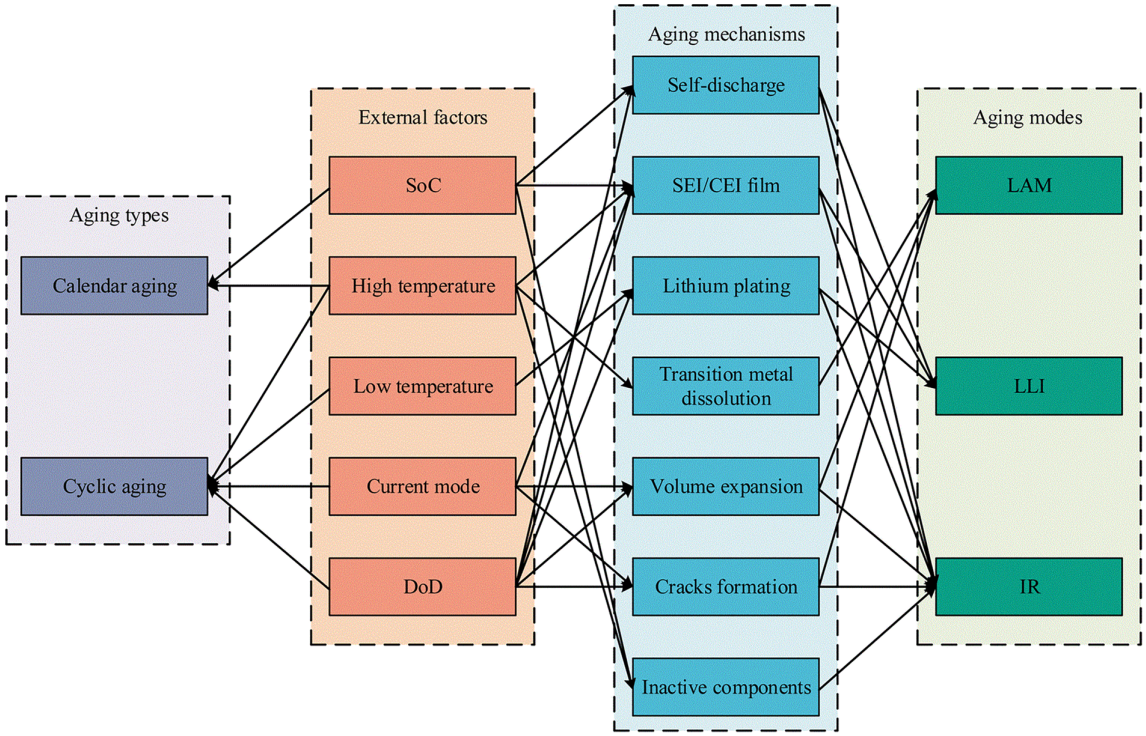


FIGURE 5 Influencing factors on aging side reactions and the corresponding aging types.[27]

While the capacity reduction with time and temperature during storage characterizes calendar aging, repeated charge–discharge cycles cause irreversible capacity losses, that is, cycle aging. Evaluating the effects of different external stresses on aging may make it easier to build accurate prognostic models (reliable operating curves) for battery life extension, as shown in Figure 5. While high temperature and SOC accelerate calendar aging, the effect of temperature is more dominant than SOC and causes more overpotentials at the electrode/electrolyte interface. The available operating mode (waveform, current rate, etc.), ambient temperature, depth of discharge (DOD), and average SOC affect cycle aging. A high current rate increases lithium ions deposited on the anode surface and accelerates aging. A dynamic pulse current and multistep constant current cycling can extend battery life due to the stable nature of the SEI. On the other hand, an ambient temperature below or above 25°C is not desirable due to accelerated aging. At temperatures below this, LLI becomes the main cause of aging in pouch cells and strengthens LAM by inhibiting intercalation kinetics. Rising DOD continuously increases the aging speed and accounts for the unpredictable nature of aging as electrode materials differ in their sensitivity to changes in DOD and SOC.

4 | BATTERY AGING ANALYSIS METHODS

Estimating battery capacity degradation over time is an ongoing and still unpredictable phenomenon. In general, DOD, SOC, charge, and discharge rate (C-rate), and hence current represent internal factors in battery degradation, while temperature and time refer to external factors.[28] The aging period still needs to be determined, depending on the battery application area, chemistry, and manufacturer.[29] It has also been suggested that a C-rate below one has little effect on the battery capacity lost, and therefore, the effects on cycle life are negligible.[30,31] Self-discharge is usually neglected in capacity losses due to aging in Li-ion batteries.[32] On the other hand, Figure 6 shows how to estimate the battery's state of health (SOH) for degradation or aging characteristics such as loss of capacity and internal resistance measurement. The SOC and SOH for the state of healthy cells are frequently used predictive indicators. Experimental, model-based, and machine-learning methods are available for SOH estimation based on expected lifetime and performance. Experimental techniques in the direct measurement category include impedance, capacitance testing, internal resistance, and AC/DC testing. In contrast, non-direct categories include incremental capacitance

25784862, 2024, 4, Downloaded from https://onlinelibrary.wiley.com/doi/10.1002/est2.661 by Yildiz Technical University, Wiley Online Library on [13/06/2024]. See the Terms and Conditions (https://onlinelibrary.wiley.com/terms-and-conditions) on Wiley Online Library for rules of use; OA articles are governed by the applicable Creative Commons License

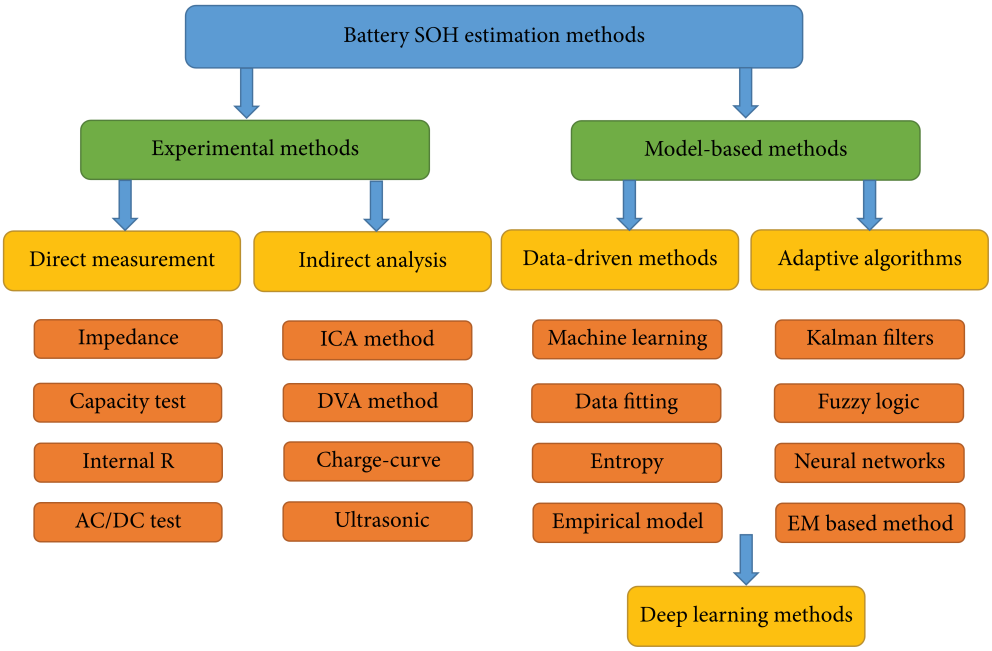


FIGURE 6 Classification of battery SOH assessment.[33]

analysis, differential voltage analysis, charge curve, and ultrasonic approaches. Model-based methods can be divided into two categories: data-driven and adaptive algorithms. Machine learning comes first to mind for data-driven methods, while data fitting, entropy, and empirical approaches are in the related category. Kalman filter, fuzzy logic, artificial neural networks, and expectation maximization-based approaches can be considered adaptive algorithms. For commercial purposes, model-based strategies fall behind, while electrochemical modeling requires the solution of multiple differential equations. Historical data is not always available for machine learning.[33]

In conventional internal resistance measurement, the two main contributions to the internal resistance of a Li-ion battery are polarization resistance and ohmic resistance.[34] The ohmic resistance represents the contact resistance due to the electrolyte, electrode material, and separator, while the polarization resistance determines the conversion between electrode and electrolyte in the electrochemical reaction. Internal resistance increases are closely related to battery capacity and discharge time. The dominant effect of SOC and temperature on internal resistance has been chiefly confirmed.[35-37] It is also emphasized that after a specific aging period, the capacity losses due to internal resistance decrease due to cycling.[38] Each cycle's internal resistance is inconsistent due to SOC, electrolyte temperature, load current, and battery capacity. Although the internal resistance can be determined with pulse strategies based on Ohm's law, it is emphasized by Schweiger et al.[39] that determining the internal resistance using energy dissipation based on Joule's law is more reliable. The approach using calorimetry for thermal loss in the charge-discharge process could not avoid costly laboratory conditions. Equation (8) is also proposed, considering electrochemical control of the temperature change in the cycle and neutralization of the reversible thermal effect. Can other methods, such as using the AC first and then the DC strategy, reduce costs in the lab? Electrochemical impedance spectroscopy (EIS) was first applied to a method where the battery does not need to be charged and discharged, keeping it at ambient temperature for a specific period. Although it performs similarly to energy loss, measuring the internal resistance's active, inductive, and capacitive components is essential. The first perspective in AC, which allows measurement across the phase angle, is easily adaptable to complex measurements. It must be accepted that the limited voltage prevents its commercial use for multicell batteries. The open circuit and cell voltage are measured at DC, and the internal resistance is calculated based on Kirchhoff's circuit law. While applicable for high-capacity batteries, the diffusion polarization-dependent method is highly sensitive. The relationship between cell temperature and impedance is found from the empirical statement (Equation 9) based on the EIS measurement for the 1 Hz impedance condition.[40,41] Equation (10) using EIS states the effect of SOC and temperature on capacity loss, which considers discharge pulses due to non-constant stress levels.[42] However, correlating the capacity loss of lithium-ion cells with $t^{1/2}$ reduces the fit quality with the data in capacity loss estimation. A decreasing degradation rate with SOH obtained a better quality fit and aging characteristics.

25784862, 2024, 4, Downloaded from https://onlinelibrary.wiley.com/doi/10.1002/est2.661 by Yildiz Technical University, Wiley Online Library on [13/06/2024]. See the Terms and Conditions (https://onlinelibrary.wiley.com/terms-and-conditions) on Wiley Online Library for rules of use; OA articles are governed by the applicable Creative Commons License

$$R_i = \frac{(C_{\text{cal}} + C_{cell}).(T_2 - T_1)}{\int_{t1}^{t2} (I_{sm}(t))^2.dt} \quad (8)$$

$$Z(1)_{\text{adj}} = Z(1)_{\text{model}} + 0.066.T_{\text{cell}}^2 - 5.362.T_{\text{cell}} + 93.52 \quad (9)$$

$$Q_{\text{loss}}(t) + \frac{1}{2}\frac{Q_{\text{loss}}(t)^2}{C_{\text{nom}}} = \frac{C_{\text{nom}}}{\alpha+1}\left[\left(1 + \frac{Q_{\text{loss}}}{C_{\text{nom}}}\right)^{\alpha+1} - 1\right] \quad (10)$$

5 | BATTERY AGING EQUATIONS

This section discusses model classification (see Section 5.1) and conventional and advanced aging equations proposed by researchers (see Section 5.2). The focus is on aging analyses and analytical/deterministic methods.

5.1 | Battery aging model

Battery degradation models are classified as linear, Peukert lifetime energy throughput (PLET), National Renewable Energy Laboratory (NREL), Arrhenius, and combined Arrhenius-Peukert-NREL (CAPN).[43] Assuming that the number of cycles until battery failure is only related to the DOD, the capacity loss in the linear model is calculated by Equation (11). Depending on the limitation of the Peukert coefficient (k_p) between 1.1 and 1.3 and the number of charges/discharges (n) over the battery lifetime considering complete and incomplete cycles, the capacity loss is as in Equation (12). Therefore, total throughput is determined via experimentation and is considered constant for any given DOD. Considering the weighted throughput-dependent aging model, NREL adopts a quadratic function of SOC as in Equation (13), although it partially reflects calendar aging. Based on the throughput in Ah, the Arrhenius-based method effectively determines the SEI film growth. The corresponding approximation can easily relate to different C-rates in time-dependent capacitance fading models. The general form discretizing in Ah is given in Equation (14). Other degradation models consider a single factor based on simplifying logic. The semi-empirical CAPN model considers the impact of each factor on battery degradation behavior. Arrhenius considers the linear effect of the C-rate on capacity degradation while integrating PLET and NREL for DOD and SOC is utilized. The linear sum of the four aging factors forms the CAPN model, as in Equation (15).

$$Q_{\text{loss}}^{\text{Linear}}(T) = \sum_{t=1}^{T}\left(\frac{1}{\frac{1}{N_{cd}}\sum_1^n Q_{\max} g_n f_n} P_{\text{ESS}}(t)\Delta t\right) \quad (11)$$

$$Q_{\text{loss}}^{\text{PLET}}(T) = \frac{1}{N_{cd}.\text{DOD}^{k_p}} \sum_{t=1}^{T} (\Delta\text{DOD}(t))^{k_p} \quad (12)$$

$$Q_{\text{loss}}^{\text{NREL}}(T) = \frac{1}{C_R D_R L_R} \sum_{t=1}^{T}\left(\left(\frac{D_A}{D_R}\right)^{u_0} e^{u_1\left(\frac{D_A}{D_R}\right)} \frac{C_R}{C_A} d_{\text{actual}}\right)_t \quad (13)$$

$$Q_{\text{loss}}^{\text{Arrhenius}}(T) = \left(A.e^{\left(\frac{-E_a}{R.T}\right)} Ah^z\right)(T-1) + z.A^{\frac{1}{z}}.e^{\left(\frac{-E_a}{z.R.T}\right)}. \left(\int_{t-1}^{t} |I_{ESS}(t)|dt\right).\left(A.e^{\left(\frac{-E_a}{R.T}\right)} Ah^z\right)(T-1)^{\frac{z-1}{z}} \quad (14)$$

$$Q_{\text{loss}}^{\text{CAPN}}(T) = \lambda_1.\left[(\alpha+\beta.C_{\text{rate}})e^{\left(\frac{-E_a}{R.T}\right)Ah^z}(T-1) + z(\alpha+\beta.C_{\text{rate}})(\alpha+\beta. C_{\text{rate}})^{\frac{1}{z}}.e^{\left(\frac{-E_a}{z.R.T}\right)\Delta Ah.(\alpha+\beta.C_{\text{rate}})e^{\left(\frac{-E_a}{R.T}\right)Ah^z}.(T-1)^{\frac{z-1}{z}}}\right] + \lambda_2.Q_{\text{loss}}^{\text{PLET}}(T) + \lambda_3.Q_{\text{loss}}^{\text{NREL}}(T) \quad (15)$$

5.2 | Battery aging equations

The correlation between the rate constant of a chemical reaction and factors such as temperature and activation energy can be analyzed via Arrhenius, as in Equation (16). This equation can be used to consider the relationship between battery capacity and power reduction with ambient temperature and time. High temperatures under accelerated aging conditions significantly impact battery health.[44] The researchers Bloom et al.[45] obtained the curve fitted in Equation (17) based on experimental results of 18 650 cells with a capacity of 0.9 Ah at temperatures higher than 40°C. While calendar aging is more related to time, in cycle aging, the battery throughput, characterized in Ah, is highly correlated with capacity degradation. Notably, the C-rate is neglected in these equations, so it is necessary to replace time with throughput in the Arrhenius equation.[46] In particular, the battery throughput is revised to reflect the number of cycles, DOD, and battery capacity. The so-called pre-exponential factor B is updated, as in Equation (18). Since neglecting the SOC reduces the accuracy, the general expression of the cycle-dependent capacity degradation was determined by Wang et al.[46] as in Equation (19).[44,47] The aging

25784862, 2024, 4, Downloaded from https://onlinelibrary.wiley.com/doi/10.1002/est2.661 by Yildiz Technical University, Wiley Online Library on [13/06/2024]. See the Terms and Conditions (https://onlinelibrary.wiley.com/terms-and-conditions) on Wiley Online Library for rules of use; OA articles are governed by the applicable Creative Commons License

TABLE 2 Dependence of pre-exponential factor to C-rate.[50]

Crate	**F**(Crate)
0.5	31 630
2	21 681
6	12 934
10	15 512

equations for repeated cycles address the same issue. However, it is crucial to determine the capacity loss for each cycle and add it to the loss in the previous cycle in Equations (20) and (21); more precisely, build the calibrated fading model thanks to the expression.[48] Equation (22) is another approach considering SOC, DOD, temperature, throughput, and cycle aging.[44] The corresponding Arrhenius-based equations assume that the C-rate and temperature act exponentially on capacity loss, while SOC is a pre-exponential factor. However, it has limitations related to battery technology and experimental conditions. The literature often uses Arrhenius formulas that appropriately determine exponential temperature dependence in aging analysis. However, the temperature for Li-ion cell properties only acts somewhat exponentially in the aging analysis.[49] The proposed cycle number as a polynomial function considering the battery cycle number (C_L) before end-of-life (EOL) is shown in Equations (23)–(25). The maximum number of cycles is determined by considering the cycle effect of each factor with the expression $Q_{cal} = k_1 t + k_2\sqrt{t}$.[49] On the other hand, the temperature and C-rate are considered on an Arrhenius basis in the electrothermal battery approach, which adopts the second-order RC model and two-state thermal model for the A123 $LiFePO_4$ cylindrical cell.[50] The proposed curve-fitted degradation characteristic is as in Equation (26). Here, the C-rate dependence of the pre-exponential factor is determined by Table 2. Another dynamic Arrhenius degradation model that considers time, temperature, depth of charge, and discharge rate was proposed by Li et al.[51] The aging model was calibrated using the least squares method after keeping the C-rate constant and obtaining the necessary formulations. This was used by Wang et al.[52] as in Equation (27).

$$Q = B.e^{\left(\frac{-E_a}{RT}\right)}.t^z \tag{16}$$

$$Q_{cyc} = B.e^{\left(\frac{-31700+370.3.C_{rate}}{RT}\right)}.Ah^{0.55} \tag{17}$$

$$lnB = 1.226.e^{(-0.2797.C_{rate})} + 9.263 \tag{18}$$

$$Q = (\alpha.\mathrm{SOC} + \beta).e^{\left(\frac{-E_a+\eta C_{rate}}{RT}\right)}.Ah^z \tag{19}$$

$$\mathrm{SOC}_{avg} = \frac{1}{Ah}\int_0^{Ah_t} \mathrm{SOC}(Ah).dAh \tag{20}$$

$$\mathrm{SOC}_{dev} = \sqrt{\frac{3}{Ah}\int_0^{Ah_t} \left(\mathrm{SOC}(Ah) - \mathrm{SOC}_{avg}\right)^2.dAh} \tag{21}$$

$$Q_{cyc} = \sum_i^N \left(\left(k_1 \mathrm{SOC}_{dev,i}.e^{\left(k_2 \mathrm{SOC}_{avg,i}\right)} + k_3\, e^{\left(k_4 \mathrm{SOC}_{dev,i}\right)}\right) e^{\frac{-E_a}{R}\left(\frac{1}{T_i}-\frac{1}{T_{ref}}\right)} \right) Ah_i \tag{22}$$

$$C_L(I_d) = k_5 e^{(k_6 I_d)} + k_7 e^{(k_8 I_d)} \tag{23}$$

$$C_L(\mathrm{DOD}) = k_9 e^{(k_{10}\mathrm{DOD})} + k_{11} e^{(k_{12}\mathrm{DOD})} \tag{24}$$

$$C_L(I_{ch}) = k_{13} e^{(k_{14} I_{ch})} + k_{15} e^{(k_{16} I_{ch})} \tag{25}$$

$$\Delta \mathrm{SOH}_k = -\frac{|I_k|\Delta t}{2\,.\,3600.\left[\frac{20}{F(\mathrm{Crate}).e^{-\frac{31700-370.3.\mathrm{Crate}}{R.T_a}}}\right]^{\frac{1}{0.55}}} \tag{26}$$

$$Q_{loss} = 0.0032.e^{\left(-\frac{15162-1516.C_{rate}}{R.(|285.75-T|+265)}\right)} Ah^{0.849} \tag{27}$$

In addition to the cycle-oriented aging properties, researchers working on calendar aging argue that calendar aging varies with the square root of time, inspired by experimental and data-fitting results.[53-55] The discrete or combined effect of linear and square root dependence of time in calendar aging can be emphasized.[56] The exponential fit function ρ is found by Marongiu et al.[57] as in Equation (28) considering the storage voltage, while the empirical model, including both calendar and cycle capacity fading, is expressed by Equations (29)–(31).[58-60] A novel approach similar to SOC considers the state of energy (SOE), where the calendar and cycle aging are as in Equations (30) and (31).[61] SOE is usually called 100% occupancy minus the available DOD.[62] Factors such as storage time, SOC, and temperature determine calendar aging. It is calculated as in Equation (32) based on the linearized approach of Mulleriyawage and Shen,[63] where the battery storage temperature is kept constant. The charging and discharging efficiency at the time step and the capacity loss due to power are determined in Equation (33). In the nonlinear aging model proposed by Amini et al.,[64] the regression method linearizes the general expression based on installation time, SOC, temperature, time interval h, and battery capacity, as in Equation (34).

25784862, 2024, 4, Downloaded from https://onlinelibrary.wiley.com/doi/10.1002/est2.661 by Yildiz Technical University, Wiley Online Library on [13/06/2024]. See the Terms and Conditions (https://onlinelibrary.wiley.com/terms-and-conditions) on Wiley Online Library for rules of use; OA articles are governed by the applicable Creative Commons License

$$Q_{\text{cal}} = \kappa.e^{\left(\frac{-\rho}{T}\right)}.e^{\lambda V}.\sqrt{t} \tag{28}$$

$$Q_{\text{total}} = (k_{12}V + k_{13})e^{\frac{k_{14}}{T}}. \\ t^{0.75} + \left[k_{15}\left(V_{\text{avg}} + k_{16}\right)^2 + k_{17}\text{DOD}\right]. \\ Ah^{0.5} \tag{29}$$

$$Q_{cal} = Q_{cal,0}.e^{\frac{SOE - SOE_0}{k_{18}}}.e^{\frac{T - T_0}{k_{19}}}\sqrt{t} \tag{30}$$

$$Q_{\text{cyc}} = \sum_{i}^{N}\left(k_{20}\Delta\text{SOE}_i^3 + k_{21}\Delta\text{SOE}_i^2 + k_{22}\Delta\text{SOE}_i\right) \tag{31}$$

$$\beta_{\text{cal}}[n] = \sum_{\tau=1}^{n}\left(6.6148.10^{-6}.\text{SOC}[n] + 4.6404.10^{-6}\right)[\tau] \tag{32}$$

$$\beta_{\text{cyc}}[n] = 0.5.\frac{\sum_{\tau=1}^{n}|P_b[\tau]|.\Delta t}{L_{\text{cyc}}E_b} \tag{33}$$

$$Q_h^{\text{cal}} = \left[\left(\frac{h}{720}\right)^{0.8} - \left(\frac{h-1}{720}\right)^{0.8}\right]. \\ \left(0.0028.\text{SOC}_h + 0.001939.E_h^{\text{BES}}\right)\forall h \in \Omega^h \tag{34}$$

Optimization tools mostly use simplified equivalent Ah-Cycle models. After a limited number of charge and discharge cycles,[65] data from battery manufacturers are generally used to determine which batteries achieve EOL. However, the lifetimes promised by battery manufacturers have yet to be completed due to the high DOD. The relationship between cycle life and DOD is proposed by Lee and Kim[66] as in Equation (35). While the ß coefficients may vary depending on the battery type/chemistry, they are obtained by the manufacturer by fitting the experimental data to the curve. The Arrhenius formula for calendar aging derived from experimental data is as in Equation (36).[67] On the other hand, acid stratification and the time during which the battery does not fully charge are not considered. In such a strategy, the overall aging characteristic is expressed by Equation (37) considering the number of complete cycles ($Z_n(t)$). Based on the Dowing algorithm, the cycle counting or rain flow methods consider the DOD and the number of cycles corresponding to the divided m intervals for the studied aging period. The number of cycles to failure, that is, replacement (CF_i), is found cumulatively by Equation (38). Various methods have been developed for this approach, which does not consider current, temperature, and acid stratification. Considering aging factors due to battery operating conditions with a weighting coefficient, researchers Schiffer et al.[68] calculate the total capacity loss due to corrosion and degradation as in Equation (39). The modeling by Petit et al.[69] proves the effect of time and temperature on capacity loss compared to DOD based on accelerated charge/discharge tests at different temperatures and DOD. Although it is known that charging and discharging current, DOD, and temperature are effective in cycle degradation,[70] it emphasizes that charging and discharging times and the standby between them should be addressed. The researchers Petit et al.[69] estimate the cycle aging considering the calendar aging mainly due to current and temperature by Equation (40). The battery capacity loss caused by calendar and cycle aging as a function of cumulative discharge, elapsed time, operating temperature, and charging current is considered by Cardoso et al.[71] as in Equation (41). The aging behavior specifically assumes a charge corresponding to a C-rate below 0.5 and operating conditions at 288–303 K. A comprehensive aging model for 18 650 lithium-ion batteries based on Li(NiMnCo)O_2 was developed by Schmalstieg et al.[58] The calendar and cyclic integrated method consider time, voltage, and temperature dependence. Moreover, the temperature and voltage function $\alpha_{\text{cap}}(T,V)$ for calendar aging and the quadratic voltage dependence and DOD variation are included in the aging with β_{cap}. The resistance rise is linear in the capacity loss due to cycling and is expressed as a net square root function. The final aging characteristic is obtained by the first formula in Equation (42), considering the effects on capacity and resistance and via the total fitness function.

$$N_{\text{cycle}} = \beta_0\text{DOD}^{-\beta_1}e^{\beta_2(1-\text{DOD})} \tag{35}$$

$$\text{CI}_{\alpha,cal} = 14.876.e^{\left(\frac{-E_a}{R.T}\right)}\psi_d(t_h)^{0.5} \tag{36}$$

$$Z_n(t+\Delta t) = Z_n(t) + \frac{\left|I_{\text{discharge}}(t)\right|.\Delta t}{C_n} \tag{37}$$

$$\text{Lifetime} = \frac{1}{\sum_{i=1}^{m}\frac{Z_i}{CF_i}} \tag{38}$$

$$C_{\text{residual}} = C_{d,0} - C_{\text{corr}}(t) - C_{\text{deg}}(t) \tag{39}$$

$$Q_{\text{loss}}^{\text{cyc}} = B_{cyc}e^{\left(\frac{-E_{a,cyc}+\gamma.I}{R.T}\right)}Ah^{Z_{\text{cyc}}} \tag{40}$$

$$Q^{T'}\left(\sum_{t'}Ah_{t'}, \overline{T}', K, i^*\right) = \left(\zeta.K^2 + \varrho.K + \varsigma\right)e^{(\gamma.K+\varepsilon)i^*}\sum_{t'}Ah_{t'} \\ + \vartheta.\varepsilon^{-\frac{E_a}{R.K}}\sqrt{\overline{T}'} \tag{41}$$

25784862, 2024, 4, Downloaded from https://onlinelibrary.wiley.com/doi/10.1002/est2.661 by Yildiz Technical University, Wiley Online Library on [13/06/2024]. See the Terms and Conditions (https://onlinelibrary.wiley.com/terms-and-conditions) on Wiley Online Library for rules of use; OA articles are governed by the applicable Creative Commons License

$$\text{Aging calculation} \;=\; > \begin{cases} C = 1 - \alpha_{\text{cap}}.t^{0.75} - \beta_{\text{cap}}.\sqrt{Q}.R = 1 + \alpha_{\text{res}}.t^{0.75} + \beta_{\text{res}}.Q \\ \alpha_{\text{cap}}(T,V) = (7.543.V - 23.75).10^{6}.e^{-\frac{6976}{T}} \\ \alpha_{\text{res}}(T,V) = (5.270.V - 16.32).10^{5}.e^{-\frac{5986}{T}} \\ \beta_{\text{cap}} = 7.348.10^{-3}.(\text{ØV} - 3.667)^{2} + 7.600.10^{-4} + 4.081.10^{-3}.\Delta\text{DOD} \\ \beta_{\text{res}} = 2.153.10^{-4}.(\text{ØV} - 3.725)^{2} - 1.521.10^{-5} + 2.798.10^{-4}.\Delta\text{DOD} \end{cases} \tag{42}$$

The SOC is found by Equation (43), considering the efficiency and power in charge and discharge and based on the battery's nominal capacity.[72] The SOC based on residual charge is usually expressed as in Equation (44), considering the cell input and output current variation by the Coulomb method.[73] This approach is a frequently used notation by researchers. The SOH term is determined by the ratio of the residual capacity to the nominal capacity.[74] A data-driven and quasi-experimental Li-NMC degradation model was considered, and the nonlinear capacity degradation (L) was derived based on the linear cycle (f) as in Equation (47).[75] 18 650 nickel–manganese–cobalt (NMC) cells were semi-experimentally tested.[76] Equation (48), whose parameters were determined by curve fitting, assumed constant cell temperature and capacity loss due to single-cell behavior. Although temperature-based functions have been developed, their reliability regarding aging characteristics is low. On the other hand, researchers often prefer linear models; the multistage battery aging model[77] stands out. Internal chemical reactions need to be included in linearized approaches that consider external stress factors, and the multistage process is developed in Equation (49). Acceleration factors corresponding to charge-discharge rates at different life phases are also considered. The gradual degradation concept and prognostic curves are considered by Russell et al.,[78] and recursive capacity estimation determines the initial capacity. The exponential loop will increase with time if the initial parameter ranges are not chosen on a narrow scale. It tends to degrade more slowly than the actual degradation characteristic. Selecting the initial ranges by curve fitting as in Equation (50) avoids the problem, while the exponential pattern can follow the degradation. This approach is sensitive to initial intervals, and degradation increases sharply in later battery life cycles. Therefore, it produces prognostic curves that do not reflect the real characteristic and should be handled carefully. Adaptively estimating the SOC,[79] the system parameters are obtained from the equivalent battery circuit consisting of two RCs and one R using the least squares method and considering the capacity degradation. While estimating the SOC with the adaptive extended Kalman filter, a capacity error model is developed to show the sensitivity of the SOC estimation to capacity degradation. The effect of the charging rate on the capacity loss needs to be addressed due to the constant and low charging rates in the charging state. The aging functions $u(T,t)$, $u(R_d,t)$, and $u(T,R_d)$ caused by stress factors under steady conditions are considered. In addition, the discharge current for EV power demand cannot be provided due to the lack of a steady operation mode. The capacity degradation and internal resistance increase under dynamic conditions are modeled by $K_{t+i}(T_{t+i},R_{d,t+i})$ as in Equation (51).

$$\text{SOC}(t) = \text{SOC}(t-1) + \frac{\left[\eta_{ch}P_{ch}(t) - \frac{P_{\text{dis}}(t)}{\eta_{\text{dis}}}\right]\Delta t}{C_n} \tag{43}$$

$$\text{SOC} = \text{SOC}_0 - \frac{1}{C_{\text{cap}}}\int_0^t \eta.I_{\text{bat}}.dt \tag{44}$$

$$Q_{\text{cal}}(t) = 0.019.\text{SOC}^{0.823} + 0.5195. \left(3.258.10^{-9}.T^{5.087} + 0.295\right).m^{0.8} \tag{45}$$

$$Q_{\text{cyc}}(t) = 0.5\left(\frac{\left|\eta_{ch}P_{ch}(t) - \frac{P_{\text{dis}}(t)}{\eta_{\text{dis}}}\right|\Delta t}{L_{\text{cyc}}^{80\%}.C_n}\right) \tag{46}$$

$$L = 1 - 0.0575.e^{-121.f} - (1 - 0.0575)e^{-f} \tag{47}$$

25784862, 2024, 4, Downloaded from https://onlinelibrary.wiley.com/doi/10.1002/est2.661 by Yildiz Technical University, Wiley Online Library on [13/06/2024]. See the Terms and Conditions (https://onlinelibrary.wiley.com/terms-and-conditions) on Wiley Online Library for rules of use; OA articles are governed by the applicable Creative Commons License

$$\begin{cases} i_X^{\text{cell}}(t) = \dfrac{P_X(t)}{N_X^{\text{parallel}} N_X^{\text{series}} \left(3.679.e^{-0.1101.\text{SOC}_X(t)} - 0.2528.e^{-6.829.\text{SOC}_X(t)} + 0.9386.\text{SOC}_X(t)^2\right)} & \forall t \\ \Delta E_X^{\text{cycle}}(t) = \left(0.00054.e^{0.35.\left|i_X^{\text{cell}}(t)\right|} i_X^{\text{cell}}(t)\Delta t\right) \dfrac{E_{\text{BES}}^{\max}}{100} & \forall t \\ \Delta E_X^{\text{cal}}(t) = \left(14.876.\sqrt{t}.e^{-24\text{kJ/RT}}\right) \dfrac{E_{\text{BES}}^{\max}}{100} = 2.64.10^{-4} \Delta t \dfrac{E_{\text{BES}}^{\max}}{100} & \forall t \\ \Delta E_X^{\text{tot}} = \sum_{t=0}^{N} \left(\Delta E_X^{\text{cycle}}(t) + \Delta E_X^{\text{cal}}(t)\right) & \end{cases} \tag{48}$$

$$\text{Aging Model} = \begin{cases} \text{Linearized Function} = L^{\text{com}} = \begin{cases} \dfrac{\kappa_D \eta_c P^{ec} \Delta t}{E_{\max}} + \kappa_{\text{cal}} \Delta t & \text{charging} \\ \dfrac{\kappa_D P^{ed} \Delta t}{\eta_d E_{\max}} + \kappa_{\text{cal}} \Delta t & \text{discharging} \end{cases} \\ \text{Multistage Function} = L_l^{\text{com},m} = \begin{cases} \dfrac{\kappa_1^D \eta_c P^{ec} \Delta t}{E_{\max}} \left(a_{m_{p,l}} \dfrac{P^{ec}}{P_{\text{rated}}} + b_{m_{p,l}}\right) + \chi_1 \kappa_1^{\text{cal}} \Delta t & \text{charging} \\ \dfrac{\kappa_1^D P^{ed} \Delta t}{\eta_d E_{\max}} \left(a_{m_{p,l}} \dfrac{P^{ed}}{P_{\text{rated}}} + b_{m_{p,l}}\right) + \chi_1 \kappa_1^{\text{cal}} \Delta t & \text{discharging} \end{cases} \end{cases} \tag{49}$$

$$x_k = x_{k-1} - \frac{\text{r.f.k}}{10\,000 + (\text{f.k})^2} + v_p \tag{50}$$

negligible effect on battery power,[81] but mechanical stresses and side reactions reduce cycle life due to

$$\begin{cases} u(T,t) = e^{\left[17.4 - \frac{4330.2}{T}\right].t^{0.79}}; & \text{static conditions} \\ \text{u}(R_d,t) = \left(2.66.R_d^{2.035} + 11.33\right).t^{0.79}; & \text{static conditions} \\ \text{u}(T,R_d) = e^{\left[4330.2.\left(\frac{1}{293} - \frac{1}{T}\right)\right]}.\left(2.66.R_d^{2.035} + 11.33\right).t^{0.79}; & \text{static conditions} \\ K_{t+i}(T_{t+i},R_{d,t+i}) = e^{\left[4330.2.\left(\frac{1}{293} - \frac{1}{T_{t+i}}\right)\right]}.\left(2.66.R_{d,t+i}^{2.035} + 11.33\right); & \text{dynamic conditions} \end{cases} \tag{51}$$

Differently, the relationship between battery capacity and temperature must first be empirically explained as in Equation (52) to analyze the effects of DOD on battery loss capacity and cycle life.[29] Higher temperatures increase SEI accumulation, rapidly decreasing the cycle life.[45,80] The relationship between cycle life and temperature is described by Zia et al.[29] as in Equation (53). In contrast to temperature, DOD has a DOD. The logarithmic model in Equation (54) explains DOD's impact on cycle life.[29] Accordingly, it can be emphasized that DOD and temperature, higher C-rate, frequent cycling, and high/low storage stresses are effective in cycle aging. Operation at high temperature and SOC can also significantly affect calendar aging.[82,83] The dependence of cycle aging on cumulative throughput defined by pre-exponential

25784862, 2024, 4, Downloaded from https://onlinelibrary.wiley.com/doi/10.1002/est2.661 by Yildiz Technical University, Wiley Online Library on [13/06/2024]. See the Terms and Conditions (https://onlinelibrary.wiley.com/terms-and-conditions) on Wiley Online Library for rules of use; OA articles are governed by the applicable Creative Commons License

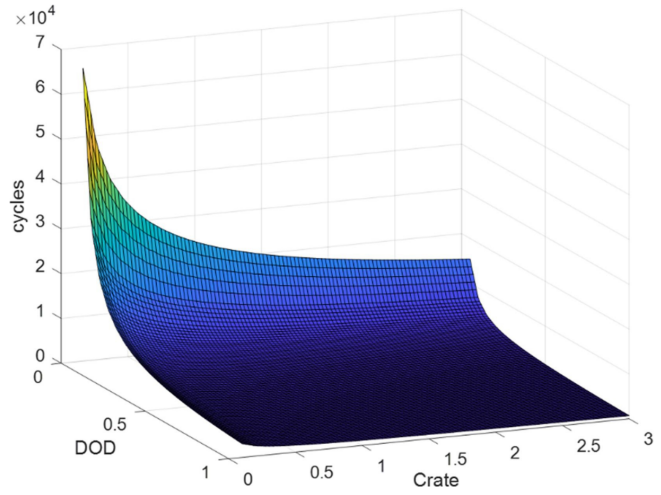


FIGURE 7 The mapping relationship between DOD, C-rate, and equivalent cycles.[84]

experimental factors (B_1 and B_2) was determined by the empirical model in Equation (55) considering $p_t^- = \sum_{i\epsilon\mathfrak{T}} P_i^- + x_{ti}$ and $p_t^+ = \sum_{i\epsilon\mathfrak{T}} P_k^+ + y_{tk}$.[62] The relationship between the cycle up to replacement and DOD was characterized by the function $f_{\mathrm{CTF}}(\mathrm{DOD})$ parameterized.[84] The effect of discharge current on battery life is determined from $f_{\mathrm{CC}}(\mathrm{Crate})$, emphasizing that a high discharge will increase battery life. The combined impact of DOD and C-rate determines the equivalent cycle life up to the replacement. The effect of DOD and C-rate on cycle life is mapped in three dimensions in Figure 7. Finally, the equivalent aging factor ($\eta(k)$) is found for each cycle, and based on the battery cycle index (k), the Rainflow counting algorithm (RCA) determines the cumulative equivalent aging index as in Equation (56).

$$h_{\Xi}(t) = -0.354.e^{-0.031.T} + 1.157 \tag{52}$$

$$h_{\zeta}(t) = -5440.35.\log(d) - 1191.54 \tag{54}$$

$$q = B_1 e^{B_2 I_c} \sum_{t\epsilon\mathcal{H}} \left(p_t^- + p_t^+\right)\Delta t \tag{55}$$

It is noteworthy that researchers frequently prefer empirical functions. Interpolation using parametric functions and determination of battery degradation is proposed by Gailani et al.[11] The experimental degradation model is shown in Equation (57), and the empirical aging characteristic obtained from the quasi-experimental case is shown in Equations (58)–(60). The capacity loss in Equation (61) is aimed to be minimized depending on Q_{SEI}, Q_{AM}, and Q_{pos}. 42 LIB cells were stored for 500 days at different temperatures and voltages to improve the repeatability and reliability of calendar aging in the empirical model. Twenty-two cycles of aging tests were performed with different DOD and average SOC to determine $C_{\mathrm{cyc}} = \beta.Nc^{0.5}$. Semi-empirical models can incorporate the neglected theoretical basis into the degradation characteristics. The empirical model captures battery cycle temperature dependence, partially reducing the need for experimental data collection. It is assumed that some of the lithium particles in the interphase between the electrolyte and the negative electrode can be prevented from contributing to SEI formation. The battery temperature dependence is captured based on the Arrhenius equation. The first term in the semi-empirical equation is the SEI layer growth, the second is the battery loss in shallow cycles, and the third is the capacity loss in the first cycle.[11] On the other hand, charging any cycle with constant current and voltage helps calculate the total charge capacity at the positive electrode, as in Equation (62).[85] Considering the side reaction at the negative electrode surface and the side reaction current (i_s) along the negative electrode length, Equation (63) expresses the total capacity lost in each charge cycle. This requires updating the SOC in the subsequent charge cycles.

$$h_{\gamma}(t) = \begin{cases} -3050.056.e^{-0.023T} + 7811.54 & -40^{\circ}\mathrm{C} \le T < 0^{\circ}\mathrm{C} \\ 14.964.T + 4767.474 & 0^{\circ}\mathrm{C} \le T < 18^{\circ}\mathrm{C} \\ -6.99.T + 5169.082 & 18^{\circ}\mathrm{C} \le T < 50^{\circ}\mathrm{C} \\ -149.889.e^{-0.117(T-50)} + 4981.68 & 50^{\circ}\mathrm{C} \le T \le 80^{\circ}\mathrm{C} \end{cases} \tag{53}$$

25784862, 2024, 4, Downloaded from https://onlinelibrary.wiley.com/doi/10.1002/est2.661 by Yildiz Technical University, Wiley Online Library on [13/06/2024]. See the Terms and Conditions (https://onlinelibrary.wiley.com/terms-and-conditions) on Wiley Online Library for rules of use; OA articles are governed by the applicable Creative Commons License

$$\text{Battery aging} = > \begin{cases} \text{CTF} = f_{\text{CTF}}(\text{DOD}) = 4.254.10^{43}.e^{-\frac{\text{DOD}-(-10.16)^2}{1.07}} + 2.134.10^{29}.e^{-\frac{\text{DOD}-(-63.13)^2}{8.235}} \\ \text{Cap}R = f_{\text{CC}}(\text{Crate}) = 0.9032 + 0.097.e^{-\frac{\text{Crate}-(-0.064)^2}{-1.378}} \\ \text{CTF}_E = f_{\text{CTF}}(\text{DOD}).f_{\text{CC}}(\text{Crate}) \\ \eta(k) = \dfrac{1}{\text{CTF}_E(k)} \\ \text{TBA} = \sum_{k=1}^{k=n} \eta(k) \end{cases} \tag{56}$$

$$C_{\text{lost1}} = (7.543.V_b(t) - 23.75).10^{-6}.e^{-\frac{6976}{T}}. \\ d^{0.75} + \beta(\text{DOD}, V_{\text{mean}}(t))\sqrt{\int 2I_b(t)} \tag{57}$$

$$Q_{\text{SEI}} = d0_{T_{(t)}}.\Big(b_0 - b_1.(T(t), \text{SOC}(t,T), \text{DOD}). \\ d^{0.5} - b_2.(T(t), \text{OCV}(t,T), \text{DOD}). \\ N_c - b_3\Big(T(t).\Big(1 - e^{-\frac{d}{\tau_{b_3}}}\Big)\Big)\Big) \tag{58}$$

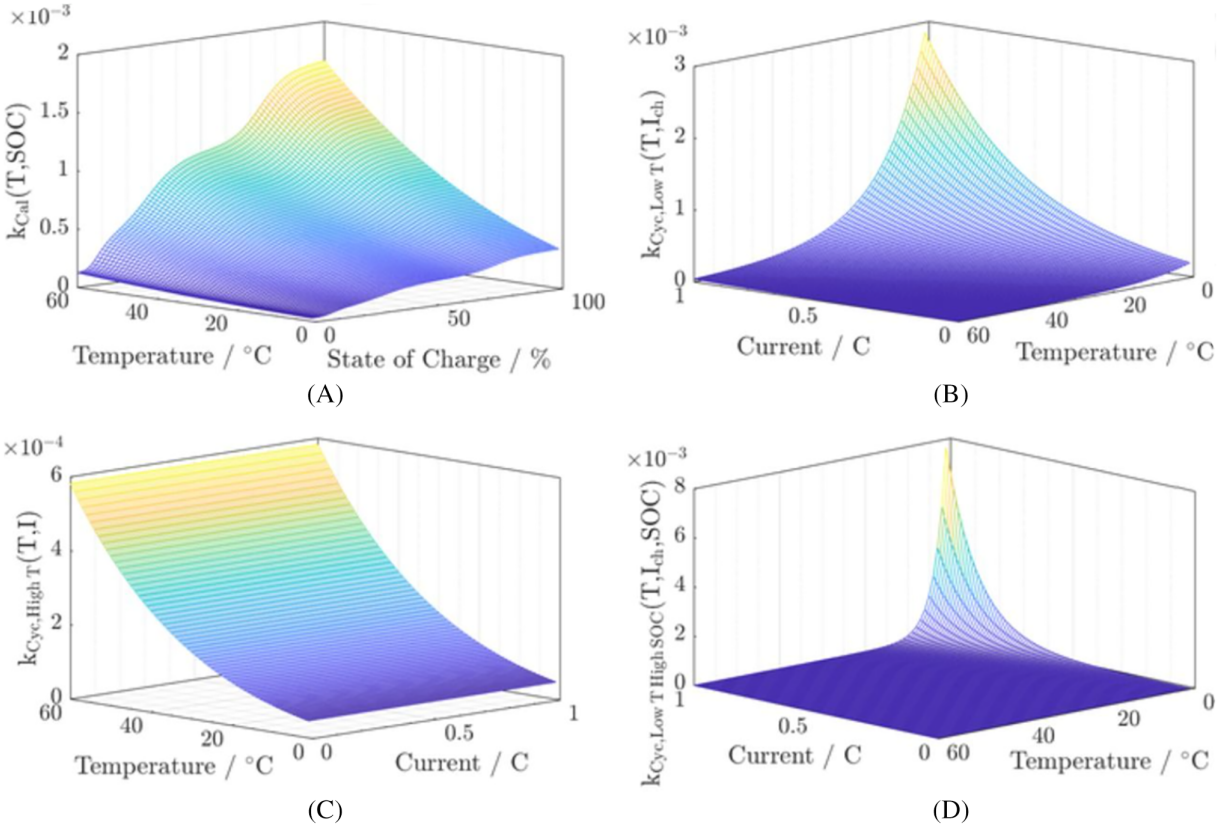


FIGURE 8 Overview of model stress factors: (A) Calendar stress factor with temperature and SOC dependence (Unit: $h^{-0.5}$), (B) cycle stress factor for low-temperature effects with charge current and temperature dependence (Unit: $Ah^{-0.5}$), (C) cycle stress factor for high-temperature effects with temperature dependence (Unit: $Ah^{-0.5}$), and (D) cycle stress factor for low temperature/high state of charge effects with charge current rate and temperature dependence (Unit: Ah^{-1}).[86]

25784862, 2024, 4, Downloaded from https://onlinelibrary.wiley.com/doi/10.1002/est2.661 by Yildiz Technical University, Wiley Online Library on [13/06/2024]. See the Terms and Conditions (https://onlinelibrary.wiley.com/terms-and-conditions) on Wiley Online Library for rules of use; OA articles are governed by the applicable Creative Commons License

$$\frac{dQ_{\mathrm{AM}}}{dN_c} = -\frac{c_1(T(t),\mathrm{DOD})}{Q_{\mathrm{AM}}} \tag{59}$$

$$Q_{\mathrm{pos}} = d0_{T_{(t)}} + \left(d_3 \left[1 - e^{\left(- \int \frac{2I_b(t)}{228} \right)} \right] \right) \tag{60}$$

$$C_{\mathrm{lost2}} = \min\left(Q_{\mathrm{SEI}}, Q_{\mathrm{AM}}, Q_{\mathrm{pos}}\right) \tag{61}$$

$$Q_P = \int 0t = T_{\mathrm{CC+CV}} \varepsilon_p \sigma_p \left. \frac{\partial \phi_1}{\partial x} \right|_{x=L_P} dt \tag{62}$$

$$\theta_1 = \frac{-\int 0t = T_{\mathrm{CC+CV}} \int 0 L_n J_s dx.dt}{Q_{\max}} \tag{63}$$

due to lithium loss in cells operated at high SOC levels is determined by the function $k_{\mathrm{Cyc,High}\ T}(T,I)$ (see Figure 8C). The current rate dependence $k_{\mathrm{Cyc,Low}\ T}(T,I_{ch})$ at low temperatures is expressed as an exponential correlation of nominal cell capacity and current (see Figure 8B). The stress factor $k_{\mathrm{Cyc,Low}\ T\ \mathrm{High\ SOC}}(T,I_{ch},\mathrm{SOC})$ is only determined from experimental data from tests above the SOC limit (see Figure 8D). Finally, the capacity loss Q_{Loss} is determined by the model parameters in Equation (64), and its relationship with the stress factors in battery aging is summarized in Figure 8. On the other hand, the temperature dependence is expressed by Arrhenius in the degradation model.[87] The Tafel equation is similarly considered to manage the open circuit voltage dependence and, hence, the electrode's nonreversible behavior. The effect of the DOD on the ΔDOD is known as the Wöhler dependence. In the approach focusing on cycle life relative to the number of cycles, the Wöhler dependence is included in Equation (65).

$$\begin{cases} k_{\mathrm{Cal}}(T,\mathrm{SOC}) = k_{\mathrm{Cal,Ref}}.e^{-\frac{E_{a,\mathrm{Cal}}}{Rg}\left(\frac{1}{T}-\frac{1}{T_{\mathrm{ref}}}\right)}.e^{\left(\left[\frac{\alpha.F}{Rg}\left(\frac{U_{a,\mathrm{Ref}}-U_a(\mathrm{SOC})}{T_{\mathrm{ref}}}\right)\right]+k_0\right)} \\ k_{\mathrm{Cyc,High}\ T}(T) = k_{\mathrm{Cyc,High}\ T,\mathrm{Ref}}.e^{\left[\frac{E_{a,\mathrm{Cyc,Low}\ T}}{Rg}\left(\frac{1}{T}-\frac{1}{T_{\mathrm{ref}}}\right)\right]} \\ k_{\mathrm{Cyc,Low}\ T}(T,I_{ch}) = k_{\mathrm{Cyc,Low}\ T,\mathrm{Ref}}.e^{\left[\frac{E_{a,\mathrm{Cyc,Low}\ T}}{Rg}\left(\frac{1}{T}-\frac{1}{T_{\mathrm{ref}}}\right)\right]}.e^{\left[\beta_{\mathrm{Low}\ T}\frac{I_{Ch}-I_{Ch,\mathrm{Ref}}}{C_0}\right]} \\ k_{\mathrm{Cyc,Low}\ T\ \mathrm{High\ SOC}}(T,I_{ch},\mathrm{SOC}) = k_{\mathrm{Cyc,Low}\ T\ \mathrm{High\ SOC,Ref}}.e^{\left[\frac{E_{a,\mathrm{Cyc,Low}\ T\ \mathrm{High\ SOC}}}{Rg}\left(\frac{1}{T}-\frac{1}{T_{\mathrm{ref}}}\right)\right]}.e^{\left[\beta_{\mathrm{Low}\ T\ \mathrm{High\ SOC}}\frac{I_{Ch}-I_{Ch,\mathrm{Ref}}}{C_0}\right]}\left(\frac{sgn\left(SOC-SOC_{ref}\right)+1}{2}\right) \\ Q_{\mathrm{Loss}} = \int k_{\mathrm{Cal}}(T,\mathrm{SOC}).\left(2\tau^{0.5}\right)^{-1}d\tau + \int k_{\mathrm{Cyc,High}\ T}(T).\left(2\varphi^{0.5}\right)^{-1}d\varphi_{\mathrm{Tot}} + \int k_{\mathrm{Cyc,Low}\ T}(T,I_{ch}).\left(2\varphi^{0.5}\right)^{-1}d\varphi_{Ch} + k_{\mathrm{Cyc,Low}\ T\ \mathrm{High\ SOC}}(T,I_{ch},\mathrm{SOC}).d\varphi_{Ch} \end{cases} \tag{64}$$

On the other hand, the temperature-dependent degradation mechanism for commercial 26 650 format $LiFePO_4$ batteries has been studied at different SOC levels through lifetime tests considering the electrochemical reactions in the battery.[86] The permanent confinement of lithium at the anode due to SEI realizes the loss of convertible lithium. Increasing the SEI thickness allows the reaction to slow down on its own. This forms the basis for calendar aging. Analyzing the impacts of SOC relative to the current requires using Tafel equations. Accordingly, $k_{\mathrm{Cal}}(T,\mathrm{SOC})$ can be determined (see Figure 8A). A superposition method is used since the capacity loss measured in cycle aging tests includes calendar aging. Deeper cycles are not directly related to increased capacity reduction. The additional capacity loss

$$\frac{dQ}{dt} = Q_e e^{\left(-\frac{E_a}{R}\left(\frac{1}{T(t)}-\frac{1}{T_{\mathrm{ref}}}\right)\right)} = Q_e e^{\left(-\frac{M.F}{R}\left(\frac{\mathrm{OCV}(t)}{T(t)}-\frac{\mathrm{OCV}_{\mathrm{ref}}}{T_{\mathrm{ref}}}\right)\right)} = \left(\frac{\Delta\mathrm{DOD}}{\Delta\mathrm{DOD}_{\mathrm{ref}}}\right)^{\hbar}$$
$$\left(\frac{dQ}{dt}\right) = \left(\frac{dQ}{dt}\right)_{\mathrm{ref}}.\left(\frac{dQ}{dt}\right)_T.\left(\frac{dQ}{dt}\right)_{\mathrm{OCV}}.\left(\frac{dQ}{dt}\right)_{\Delta\mathrm{DOD}} \tag{65}$$

Unlike lithium-ion chemistry, SOC and discharge current are considered in cycle aging for lead-acid batteries.[88] The weighted cycle number $(Z_W(t))$ is suggested by Equation (66). The expression $f_{\mathrm{acid}}(\tau) = 1 + f_{\mathrm{strat}}\sqrt{\frac{I_{\mathrm{ref}}}{|I(\tau)|}}$ details the effect of acid stratification on the weighted cycle in lead-acid batteries. The film formed on the electrode due to cell oxidation increases the internal resistance of the lithium-ion battery. Equation (67) can be used to determine the side reaction rate relationship with

25784862, 2024, 4, Downloaded from https://onlinelibrary.wiley.com/doi/10.1002/est2.661 by Yildiz Technical University, Wiley Online Library on [13/06/2024]. See the Terms and Conditions (https://onlinelibrary.wiley.com/terms-and-conditions) on Wiley Online Library for rules of use; OA articles are governed by the applicable Creative Commons License

a linear approximation of the film growth. Defining the temperature history of previous cycles and using the probability distribution ($P(T')$) to determine the film resistance is necessary. In this way, the capacity reduction can be estimated.[89] On the other hand, besides the chemical point of view, calendar aging is expressed in Equation (68) as a function of SOC, throughput, and temperature. The average cycle degradation as a function of battery discharge power and capacity is explained by Rezaeimozafar et al.[90] A different perspective is developed by Liu et al.[91] via the basic Wiener process. The Wiener process is given in Equation (69), where $Y(t)$ is the value of the quality characteristic of the battery capacity at time t. The degradation process under the charge/discharge cycle is revised by $\Delta Y(t)$after calendar and cycle aging. The traditional Wiener method is enhanced to a monotonic spline-based Wiener process mode, and an integral-based aging function is proposed. In contrast, Dakin's degradation method calculates calendar aging based on the SOC in Equation (70). The cycle degradation is calculated based on the options $a(T)$ and is Arrhenius weighted.[92] Calendar aging based on storage time, temperature, and SOC can be obtained from accelerated lifetime tests. The degradation in power capacity is more noticeable at 20% and 80% SOC compared to 50% SOC. An empirical cycle degradation function can also be obtained by considering the number of cycles (nc), temperature, and cycle depth (cd). Accordingly, Equation (71) was proposed by Swierczynski et al.[93] The linearized capacity degradation for 25°C and 180 months (15 years) lifetime depends on SOC as in Equation (72).[72] Also, the cycle degradation can be calculated from the relevant equations using the equivalent full cycle (EFC).

$$Z_W(t)=\frac{1}{C_N}\int_0^t |I_d(\tau)|\left[1+\left(c_{\mathrm{SOC},0}+c_{\mathrm{SOC,min}}\left(1-(\mathrm{SOC}_{\min}(\tau))\right)\right|_{t_0}^{t}\right)$$

$$\times f_I(t)(\tau-\tau_0)]\left(1+f_{\mathrm{strat}}\sqrt{\frac{I_{\mathrm{ref}}}{|I(\tau)|}}\right) \tag{66}$$

$$\begin{cases} \dfrac{\partial\delta}{\partial t}=\dfrac{i_k M}{L\alpha\rho F} \\ r_f(\eta_c,T')=\eta_c\displaystyle\sum_{T'}P(T').k.e^{\left(-\frac{e}{T}+\psi\right)} \\ b_1(i,T).c^{b_2(i,T)}=1-e^{\left(\frac{r(i,T,\eta_c,T').i-\left(V_{\mathrm{oc_{init}}}-v\right)}{\frac{2RT}{nF}}\right)} \end{cases} \tag{67}$$

$$\begin{cases} D_{\mathrm{cal},t}=\left(0.019.\mathrm{SOC}^{0.823}+0.5195\right). \\ \left(3.258.10^{-9}\mathrm{temp}^{5.087}+0.295\right). \\ m^{0.8} \\ D_{\mathrm{cyc},t}=0.5\dfrac{\sum_t|P_{b,t}|\Delta t}{\eta_{\mathrm{cyc}}E_b^{\max}}10^2 \\ D_{\mathrm{tot},t}=D_{\mathrm{cyc},t}+D_{\mathrm{cal},t} \end{cases} \tag{68}$$

$$\begin{cases} Y(t)=Y_0+vt+\sigma\mathrm{B}(t) \\ \Delta Y(t)=Y(t+\Delta t)-Y(t)\sim\mathcal{N}\left(\lambda_0\Delta t_0+\lambda_a\Delta t_a,\sigma_0^2\Delta t_0\right. \\ \qquad \left.+\sigma_a^2\Delta t_a\right) \\ Y(t)=\displaystyle\int_0^t\beta^{\mathrm{T}}I(x_\tau)d\tau+\sigma_a\mathrm{B}(t) \end{cases} \tag{69}$$

$$\begin{cases} k_{\mathrm{Calendar}}=\dfrac{1}{\Delta\mathrm{SOC}}\displaystyle\int_{\mathrm{SOC}_{\min}}^{\mathrm{SOC}_{\max}}\exp^{\frac{c.\mathrm{SOC}}{a}}.\exp^{\frac{d}{a}}.\exp^{\left(-\frac{b}{aT}\right)}.d\mathrm{SOC} \\ k_{\mathrm{Cyc}}=a(T)\dfrac{I}{I_0} \\ a(T)=a_1T+b_1\ \text{or}\ \dfrac{a_2}{RT}+b_2\ \text{or}\ \exp^{\left(\frac{a_3}{RT}+b_3\right)} \end{cases} \tag{70}$$

$$\begin{cases} P_{\mathrm{FADE}}(t,T,\mathrm{SOC}_{st})=\dfrac{0.000375.\mathrm{SOC}_{st}+0.1363}{0.155}.0.003738.\exp^{0.06778.T}.t \\ P_{\mathrm{FADE}}(nc,T,cd)=0.00024.\exp^{0.02717.T}.0.02982.cd^{0.4904}.nc^{0.5} \\ P_{\mathrm{FADE}}(nc,T,cd)=\dfrac{1}{3}\left(5.78.10^{-4}\exp^{0.03.T}+1.22.10^{-7}\right).2.918.10^{-5} \\ .\exp^{0.08657.cd}.nc^{(0.00434.T-0.008.cd-0.1504)} \end{cases} \tag{71}$$

$$\begin{cases} \mathrm{AGE}_{\mathrm{cal}}(t)=6.6148.10^{-6}.\mathrm{SOC}(t)+4.6404.10^{-6} \\ \mathrm{EFC}(t)=0.5\dfrac{|\eta_{ch}P_{ch}(t)-P_{\mathrm{disch}}(t)/\eta_{\mathrm{disch}}|\Delta t}{\mathrm{Cap}_{\mathrm{bat}}} \\ \mathrm{AGE}_{\mathrm{cyc}}(t)=\dfrac{\mathrm{EFC}(t)}{L_{\mathrm{cyc}}^{80\%}} \end{cases} \tag{72}$$

6 | BATTERY DEGRADATION COST AND EQUATIONS

Degradation costs need to be included in operating costs. Batteries have a complex cost function due to variations in degradation rates depending on the load profile and differences in cell chemistries and technologies. Neglecting this will hinder reliable investment plans and reduce interest in battery energy storage alternatives. Figure 9 illustrates the cost of battery degradation.

The 10°C to 50°C limits should not be exceeded in lithium-ion battery operation. If exceeded, the aging process is accelerated due to thermal management. Increasing temperature has a dominant effect on battery discharge capacity. Higher DOD, especially at low temperatures, significantly increases battery degradation costs, as seen in Figure 10. Lower degradation costs can be obtained at 60% DOD and temperatures above 10°C.[29]

On the other hand, the battery degradation cost can be expressed as in Equation (73) depending on the DOD.[94] The

25784862, 2024, 4, Downloaded from https://onlinelibrary.wiley.com/doi/10.1002/est2.661 by Yildiz Technical University, Wiley Online Library on [13/06/2024]. See the Terms and Conditions (https://onlinelibrary.wiley.com/terms-and-conditions) on Wiley Online Library for rules of use; OA articles are governed by the applicable Creative Commons License

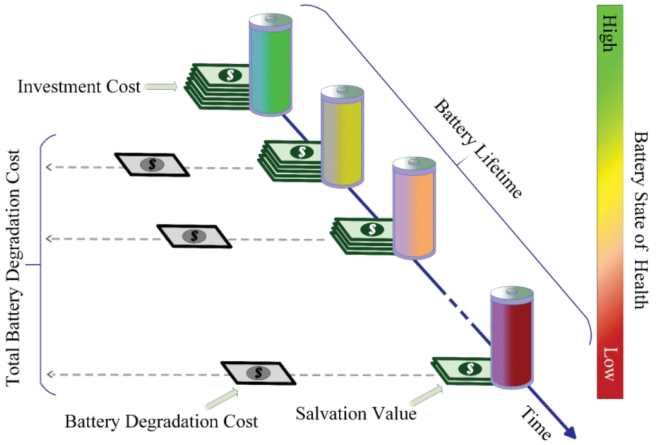


FIGURE 9 Schematic illustration of the battery degradation cost concept.[64]

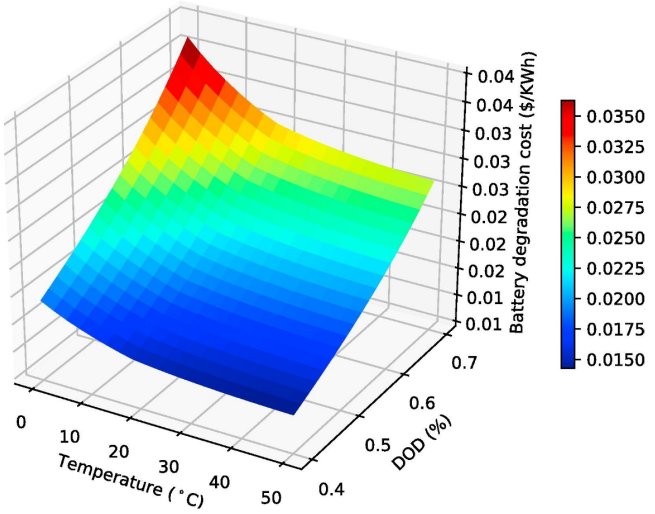


FIGURE 10 Effects of temperature and DOD on Li-ion battery degradation cost.[29]

degradation cost is evaluated by Equation (74) using lifetime throughput, DOD, and time to failure from manufacturer catalogs.[95] If the effects of temperature on cycle life and capacity loss are also considered, the battery degradation cost based on the discount rate and annual lifetime (n) is given in Equation (75).[29] The degradation is closely related to cycle-based DOD and is considered by Antoniadou-Plytaria et al.[62] as in Equation (76). Although calendar life and cycle life are not independent, Lee and Kim[66] focused on the cost due to cycle degradation in a specific operational period. Monetary factors such as interest and inflation are not considered separately as they are not operational. Accordingly, the degradation cost proposed in Equation (77) is deemed to be an unreliable function. The effects of charge and discharge cycles on degradation are independent of the previous cycle. In contrast, cell

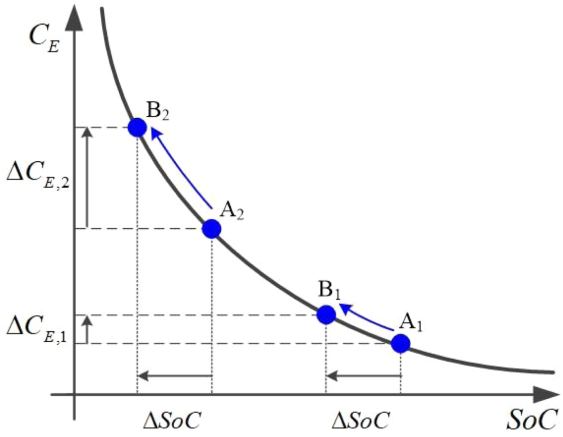


FIGURE 11 One-cycle degradation cost curve.[66]

degradation is evenly distributed up to the maximum allowable charge and discharge cycle for a particular DOD. The cost of a single cycle increases rapidly for low SOC operations, and 100% SOC can only sometimes be obtained with a full cycle. The RCA should be considered for random SOC profiles. Figure 11 shows how the single cycle degradation cost based on ΔSOC ranges can be calculated based on RCA. Complete and incomplete cycles are considered in Figure 12.[66,96]

$$\text{Cost}^{t}_{\text{deg}} = \frac{C_n.\text{DOD}.E_{\text{bat}}}{1331.\text{DOD}^{-1.825}} \tag{73}$$

$$C_{\text{O\&M}}(t) = \frac{\text{Cost}_{\text{bat}}.P_{\text{dis}}}{2.\left(\text{DOD}.\text{Cycle}_{\text{rep}}\right)_{\text{ave}}.\eta_{\text{dis}}.\eta_{\text{conv}}} \tag{74}$$

$$C^b = \frac{1}{2}\frac{\left[C^b_{\text{inv}} + \sum_{i=1}^{n} C^b_{\text{O\&M}}(1-dr)^{-i}\right](1+dr)^n - RV}{(1+dr)^n X_T^{\Xi} X_T^{\gamma} X_d^{\gamma} \gamma_{\text{ref}} \Xi_{\text{ref}}} \tag{75}$$

$$C^b = \sum_{t\epsilon\mathcal{H}} \max\left\{0, (p_t - p_{t-1}).\frac{(100\% - \eta)C^{b,0}}{B_1 e^{B_2 I_c} \sum_{t\epsilon\mathcal{H}} (p_t^- + p_t^+)\Delta t}\right\} \tag{76}$$

The controllability of cycle depth in aging characteristics is utilized[97] by considering load frequency control. Using the battery cycle depth model, the total capacity life loss considers the discrete life analysis over all discharge cycles. Equation (78) is also used for real-time cost estimation. The quadratic cycle depth voltage function $[5.24.E-4].\delta^{2.03}$ is also considered. The unplanned linearized cost in batteries and systems due to frequency deviation is estimated by Equation (79). Considering the power imbalance relative to the price differential and

25784862, 2024, 4, Downloaded from https://onlinelibrary.wiley.com/doi/10.1002/est2.661 by Yildiz Technical University, Wiley Online Library on [13/06/2024]. See the Terms and Conditions (https://onlinelibrary.wiley.com/terms-and-conditions) on Wiley Online Library for rules of use; OA articles are governed by the applicable Creative Commons License

$$C_E \approx \sum_{si}\left(X_t^{si} C_E\left(\mathrm{SOC}_{\min}+(si-1)\frac{\mathrm{SOC}_{\max}-\mathrm{SOC}_{\min}}{N_{\mathrm{seg}}}\right)\right) + \left(\frac{\left(C_E\left(\mathrm{SOC}_{\min}+\frac{\mathrm{SOC}_{\max}-\mathrm{SOC}_{\min}}{N_{\mathrm{seg}}}si\right)-C_E\left(\mathrm{SOC}_{\min}-\frac{\mathrm{SOC}_{\max}-\mathrm{SOC}_{\min}}{N_{\mathrm{seg}}}(si-1)\right)\right)}{\frac{\mathrm{SOC}_{\max}-\mathrm{SOC}_{\min}}{N_{\mathrm{seg}}}}\mathrm{SOC}_t^{si}\right) \tag{77}$$

elaborating on the relationship between battery performance and aging according to the system frequency provides a unique cost function.

$$c(t)=sgn[g_t(t)].\frac{g_t(t).R}{\eta.E.L}.\frac{\partial\Phi\left([5.24.E-4].\delta^{2.03}\right)}{\partial t} \tag{78}$$

$$c_u(t)=p(f).\Delta P(t)=>p(f) = \begin{cases} 0 & f\epsilon[1.006.f_0,1.02.f_0)\,Hz \\ \alpha_3+\beta_3.\Delta f & f\epsilon[0.99.f_0,1.006.f_0)\,Hz \\ \alpha_2+\beta_2.\Delta f & f\epsilon[0.984.f_0,0.99.f_0)\,Hz \\ \alpha_1 & f\epsilon[0.98.f_0,0.984.f_0)\,Hz \end{cases} \tag{79}$$

The partial function of the total discounted costs (TDC) for fresh and second-life batteries (FB, SLB) is expressed by Equations (80) and (81), considering the relationship between the energy and power capacity (EPR) of the system.[98] A detailed explanation of SLBs is given in Section 7. The costs in the first time step characterize the total capital costs, while the remaining costs are obtained as a function of the discount rate and the construction period. Factors such as reuse cost and SLB price determine the capital cost, while replacement costs and different degradation times are required due to the lower module lifetime compared to FB. The discharged energy is assumed to be zero for $t=0$ as no electricity is produced until the end of the construction period. The levelized cost of storage can be compared for both types of energy storage based on the costs.

7 | SECOND LIFE EV BATTERIES AND AGING EQUATIONS

The social and environmental impacts and costly investments during FB production, such as carbon emissions,

$$\mathrm{TDC_{FB}}=\begin{cases} \mathrm{tcc}_e.\mathrm{cap}_e & t=0 \\ \sum_{t=t_c}^{T}\frac{\mathrm{O\&M}_p.\mathrm{cap}_p}{(1+r)^{t_c+t}}+\frac{t.(1+P_{\mathrm{esc}}).P_{el}.\mathrm{EPR}.\mathrm{cap}_p.\mathrm{SOH}_i.\mathrm{DOD}.\mathrm{aod}.\left(1-a_{\mathrm{deg}}\right)^{t-t_c}}{{\eta_{rt}}^5.(1+r)^{t_c+t}} & t\geq t_c \end{cases} \tag{80}$$

$$\mathrm{TDC_{SLB}}=\begin{cases} (\mathrm{tcc}_e+rc_e-\mathrm{nmc}).\mathrm{cap}_e & t=0 \\ \sum_{t=t_c}^{T}\frac{\mathrm{O\&M}_p.\mathrm{cap}_p}{(1+r)^{t_c+t}}+\frac{t.(1+P_{\mathrm{esc}}).P_{el}.\mathrm{EPR}.\mathrm{cap}_{p_e}.\mathrm{SOH}_i.\mathrm{DOD}.\mathrm{aod}.\left(1-a_{\mathrm{deg}}\right)^{t-o_{\mathrm{deg}}-t_c}}{{\eta_{rt}}^5.(1+r)^{t_c+t}} & t\geq t_c \\ t=t_r\frac{(rc_e+rl_e).\mathrm{cap}_e}{(1+r)^{t_c+t}} & \\ \frac{t<t_r.o_{\mathrm{deg}}=0}{t\geq t_r.o_{\mathrm{deg}}=t_r} & \end{cases} \tag{81}$$

25784862, 2024, 4, Downloaded from https://onlinelibrary.wiley.com/doi/10.1002/est2.661 by Yildiz Technical University, Wiley Online Library on [13/06/2024]. See the Terms and Conditions (https://onlinelibrary.wiley.com/terms-and-conditions) on Wiley Online Library for rules of use; OA articles are governed by the applicable Creative Commons License

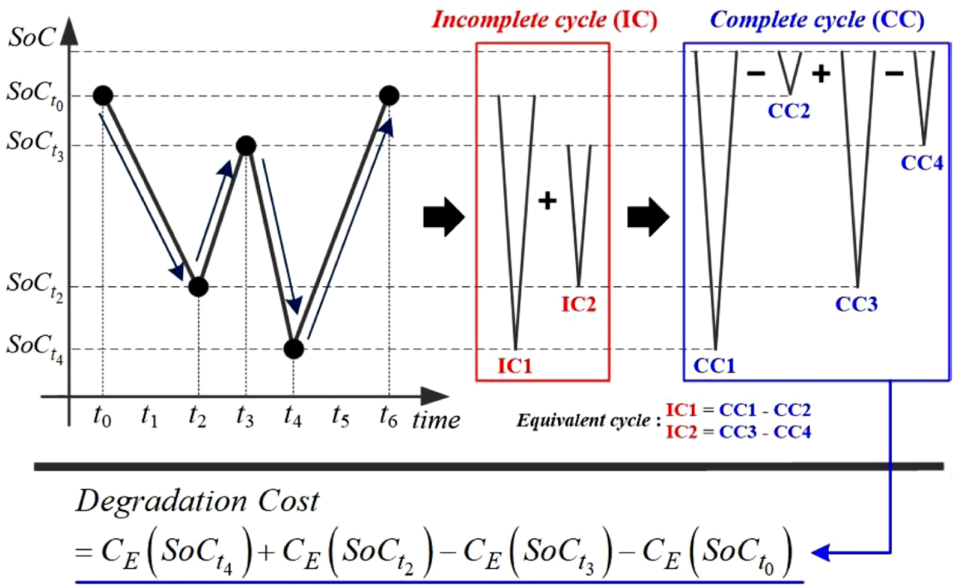


FIGURE 12 Degradation cost calculation based on complete and incomplete cycles.[66]

$$L_{\text{EES}} = \min\left(L_{\text{float}}, \frac{N_d^{\text{fail}}}{W.0.5.\sum_{t\epsilon T}\frac{\left|\left(P_{\text{EES},k}^{\wedge} - [s_t]^{-}\text{Cap}_{\text{EES},k}^{Rg}\right).\eta_{\text{EES}} + \frac{\left(P_{\text{EES},k}^{\vee} + [s_t]^{+}\text{Cap}_{\text{EES},k}^{Rg}\right)}{\eta_{EES}}\right|.\Delta t}{E_{\text{EES,rated}}}}\right) \tag{82}$$

raw material labor, water consumption, etc., require new alternatives for energy storage. It is a popular concept to consider EV batteries for second use due to their reduced capacity, increased internal resistance, and degraded performance. It is widely recognized that for SLBs, SOH drops to 70%–80% after first use. However, the state of function (SOF) and, therefore, the EOL may vary depending on the user's driving preferences, charging and discharging profile, and chemistry. The higher battery capital costs can be recouped by delaying the recycling period and extending the service life of the batteries. Carbon emissions are reduced due to the lower need for battery production. Although there is a variable cost during the second-life period, SLB purchase prices are lower than FB. The formation of a battery landfill is avoided, while the low revenues from recycling are utilized after the second use. The process and benefits from first to second use are shown in Figure 13.

In addition to lifetime extension, SLB benefits must be evaluated, especially in frequency regulation. Assuming a half cycle between two neighboring local terminals, the DOD is calculated according to the corresponding interval's dispatch strategy and regulation signal.[99] Accordingly, minimum calendar lifetime (L_{EES}) is calculated as in Equation (82), using cycle lifetime (L_{cycle}) and float lifetime (L_{float}). On the other hand, the SOH of SLB cells relative to FB is significantly heterogeneous and highly time-sensitive. The SLB discharge power for grid-level storage is low compared to its capacity, and it is emphasized that the internal resistance does not change significantly. Static semi-empirical degradation models do not reliably address life cycle analysis during variable load periods. The dynamic semi-empirical degradation model is proposed under dynamic charging and discharging conditions as in Equation (83).[100]

$$Q_{\text{loss}}(k+1) = Q_{\text{loss}}(k) + \frac{|P_{\text{bat}}(k)|.T_s}{3600.V_{\text{bat}}(k)}0.824.0.0032^{\frac{1}{0.824}}.$$
$$e^{-\frac{E_a - 1516.\frac{|P_{\text{bat}}(k)|}{V_{\text{bat}}(k).Q_{\text{bat}}(k)}}{z.R.T_{\text{bat}}}}.Q_{\text{loss}}(k)^{\frac{0.824-1}{0.824}} \tag{83}$$

25784862, 2024, 4, Downloaded from https://onlinelibrary.wiley.com/doi/10.1002/est2.661 by Yildiz Technical University, Wiley Online Library on [13/06/2024]. See the Terms and Conditions (https://onlinelibrary.wiley.com/terms-and-conditions) on Wiley Online Library for rules of use; OA articles are governed by the applicable Creative Commons License

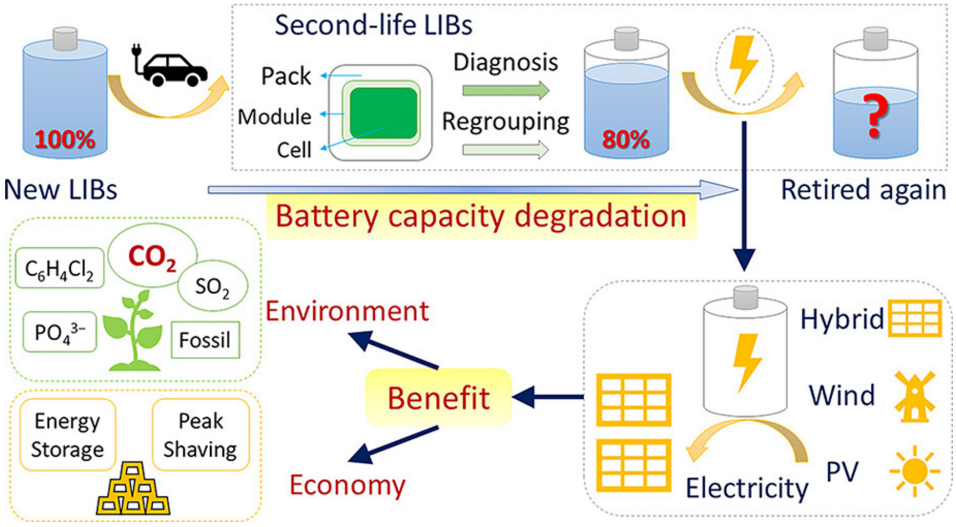


FIGURE 13 Benefits of moving to SLB.[101]

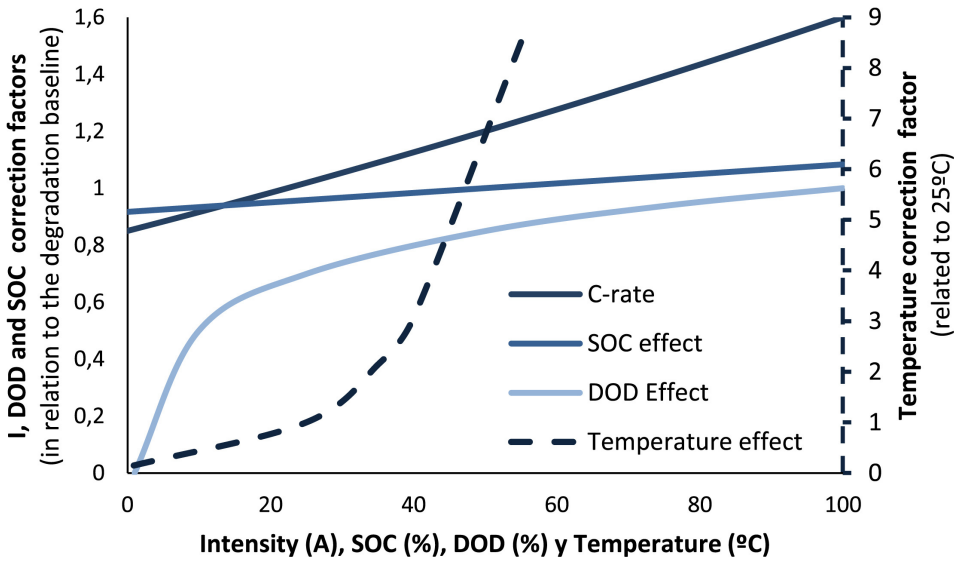


FIGURE 14 Effects of the different aging factors in relation to the baseline discharge rate at 25°C, 1C, and 100\% DOD cycles.[105]

On the other hand, researchers measure capacity degradation due to aging based on remaining useful life (RUL), while power attenuation explains impedance increase. Manufacturers provide life curves based on the number of possible cycles for constant DOD. Model-based methods use less historical data when studying the Li-ion degradation mechanism, while data-driven methods use historical data to create potential rules. Adaptive empirical equations and regression constants for SLBs were proposed by Yang et al.[102] to predict capacity degradation without requiring comprehensive testing. Different techniques can be used to fit life curves, such as least squares, Gaussian process regression, and particle swarm optimization. Exponential, polynomial, power law, and empirical formulas related to test results are also considered for curve types. Although researchers often focus on AI-based RUL estimation, impedance and capacity are difficult to obtain online. Depending on NASA datasets, degradation characteristics can serve the same purpose as conducting extensive experiments. It is argued by Swierczynski et al.[93] that the power loss for the aging period is lower than the capacity degradation, and the power and capacity loss are described in Equations (84) and (85). Another empirically fitted degradation model is expressed by Wang et al.[46] as in Equation (86). The approach is based on the exponential curve in Ah obtained by multiplying the number of cycles by the DOD and the total cell capacity. The average DOD is multiplied by the number of cycles and updated as the cycle changes. Here, the coefficients B for C/2, 2C, 6C, and 10C are assumed to be 31.63, 21.68, 12.93, and 10.51. The expression $Q_{loss} = K_f.t^{1/2}$ by Matsushima[103] focuses on the representation with the time factor. Cell degradation behavior from 100% to 70% SOH is characterized,

25784862, 2024, 4, Downloaded from https://onlinelibrary.wiley.com/doi/10.1002/est2.661 by Yildiz Technical University, Wiley Online Library on [13/06/2024]. See the Terms and Conditions (https://onlinelibrary.wiley.com/terms-and-conditions) on Wiley Online Library for rules of use; OA articles are governed by the applicable Creative Commons License

and Equation (87) is proposed. The exponential curve fitting method is adopted from He et al.,[104] and a, b, c, and d are accurately estimated in the expression $C_k = a.e^{b.k} + c.e^{d.k}$. However, DOD is not considered a parameter for capacity estimation. Therefore, it is not a valuable function for SLBs. Thus, to address this issue, Equation (88) is proposed.

$$P_{\text{fade}} = \frac{1}{3}\left(5.78.10^{-4}.e^{0.03.T} + 1.22.10^{-7}\right).2.918.10^{-5}. e^{0.08657.cd}.nc^{(0.00434.T - 0.008.cd - 0.1504)} \quad (84)$$

$$C_{\text{fade}} = 0.00024.e^{0.02717.T}.0.02982.cd^{0.4904}.nc^{0.5} \quad (85)$$

$$Q_{\text{loss}} = B.e^{\left(\frac{-31700+370.3.C_{\text{rate}}}{R.T}\right)}.Ah^{0.552} \quad (86)$$

$$Q_{\text{loss}} = \begin{cases} -0.948.t^{\frac{1}{2}} + 88.338 & @45^{\circ}\text{C} \\ -1.2906.t^{\frac{1}{2}} + 89.746 & @55^{\circ}\text{C} \\ -1.7374.t^{\frac{1}{2}} + 91.378 & @60^{\circ}\text{C} \end{cases} \quad (87)$$

$$C_k = y_1.\left(a.e^{b.y_2.k} + c.e^{d.y_2.k}\right) \quad (88)$$

Another significant issue is the ability to analyze the aging of SLBs under different stress conditions. Accordingly, a 1C charge-discharge cycle with 100% DOD, an average SOC of 50%, and a temperature of 25°C were considered.[105] In addition, the aging reference value per Ah in the cell was measured. The developed model revises the measured aging reference value based on four correction factors (C-rate, SOC, DOD, and temperature) for each moment, depending on the operating conditions. Figure 14 shows the relationship between the reference and correction factors. The effect of SOC on aging is lower than the C-rate, while the effect of temperature on aging follows an exponential curve. DOD has a logarithmic characteristic. Experimental accelerated aging tests were also used to obtain the curve. Empirical approaches based on the intuitive correlation between capacity/power decay and stress factors for aging behaviors in SLBs are focused by Ganesh and D'Arpino.[106] The correlation density is determined using the specific field strength factor, and the aging data is calibrated. This approach, limited to a particular battery chemistry, provides adequate accuracy and is helpful for online SOH estimation due to its simple structure. In contrast, some physics-based models relate the physical sub-model to the aging phenomenon, which are computationally expensive and involve many calibration parameters. They offer a more robust accuracy performance than empirical approaches. Developing the empirical approach for calibrated battery chemistries and extending the physics-based aging model with a power attenuation model considers cycle and calendar degradation as in Equation (89). The k_{SEI} and k_{LAM} for SEI layer growth and loss in active material reflect the aging mechanisms at the cell's anode. The calendar aging model is caused by the average SOC over 24 h of daily operation, and the cycle aging model uses the RCA, which was studied by Mathews et al.[75] The completion or incompletion of each cycle, cycle midpoint, start and end times, and the total number of cycles are considered. The nonlinear capacity reduction (L) due to battery cell (NMC type) life loss or operating profiles is empirically calculated as in Equation (90), assuming that the battery temperature is maintained at 25°C for both models. The loss of convertible lithium causes calendar aging, while the active material structure disruption and mechanical fracture are the actions that accelerate cycle aging.

$$\begin{cases} \frac{d\zeta}{dt^{\alpha}} = \pm\left[\left(\frac{1}{\Delta\text{SOC}}\int_{\text{SOC}_{\min}}^{\text{SOC}_{\max}} e^{\left(\frac{y_3.\text{SOC}}{y_1}\right)}.e^{\left(\frac{y_4}{y_1}\right)}.e^{\left(\frac{-y_2}{y_1.T}\right)}.d\text{SOC}\right).\left(e^{\left(\frac{y_5}{e^{R.T}}+y_6\right)\frac{I}{I_0}}\right)\right].\zeta^n \text{ Empirical model} \\ Q_{\text{loss}} = \left(\int_0^t -\frac{k_{\text{SEI}}e^{-\frac{E_{\text{SEI}}}{R.T}}}{2\sqrt{t}.(1+\lambda.\theta)}dt\right) + \int_0^t k_{\text{LAM}}e^{-\frac{E_{AM}}{R.T}}.\text{SOC}.|j_n(t)| \text{ Semi} - \text{empirical physics} - \text{based model} \end{cases} \quad (89)$$

$$L = 1 - 0.0575.e^{-121.\left(\frac{0.2}{3000.0.8^{2.03}}\delta^{2.03} + 4.1375.10^{-10}.t\right)e^{k_{\sigma}(\sigma-0.6)}e^{k_T(T-25)\frac{25}{T}}} - (1-0.0575)e^{-\left(\frac{0.2}{3000.0.8^{2.03}}\delta^{2.03} + 4.1375.10^{-10}.t\right)e^{k_{\sigma}(\sigma-0.6)}e^{k_T(T-25)\frac{25}{T}}} \quad (90)$$

The first and second discrete degradation models caused by EV driving and second-life operation are studied by Etxandi-Santolaya et al.[107] The EOL kilometers are estimated to be 344 532, considering the distances

TABLE 3 Model parameter depending on the battery capacity.[108]

Battery capacity (kWh)	ℓ	σ
16	3.64	0.000227
24		0.000161
30		0.000129
40	2.24	0.000097
70		0.000083
90		0.000064

25784862, 2024, 4, Downloaded from https://onlinelibrary.wiley.com/doi/10.1002/est2.661 by Yildiz Technical University, Wiley Online Library on [13/06/2024]. See the Terms and Conditions (https://onlinelibrary.wiley.com/terms-and-conditions) on Wiley Online Library for rules of use; OA articles are governed by the applicable Creative Commons License

traveled for the degradation due to driving, and 90% of the EV batteries are retired. The initial degradation is modeled as in Equation (91), considering aging by time (ℓ) or aging by kilometers (o). After regression analysis, the ℓ and o coefficients for the battery capacities are shown in Table 3.[108] Unlike the driving profiles, the second degradation model for NMC cells is based on the assumption of constant current discharge.[109] Considering the linear relationship between the full equivalent cycle and SOH, the complete cycle is assumed to start at 25°C, at a 1 C-rate for charge and discharge, and 100% SOC. The corresponding model is expressed in Equation (92), where SOC_m is the average SOC. The experimental data of LG Chem NMC-LMO second-life cells at 10°C, 30°C, 40°C, 45°C, 50°C, and 60°C and 30%, 65%, and 100% SoC conditions were used by D'Arpino and Cancian.[110] Based on this, the SLB capacity loss and internal resistance are calculated as in Equations (93) and (94). Between 100% and 80% SOH, that is, in the initial stages of use, the capacity lost profile shows linear behavior. However, the capacity decreases exponentially at SOH values below the second-lifetime point. C-rate is sensitively dependent on operating conditions such as charge-discharge profile and temperature. Equation (95) defines the LIB aging characteristics by Nunes et al.,[111] where the parameters a_2 and a_4 are related to the LIB's aging rate, and the corresponding coefficients are obtained from the Kalman filter.

$$SOH_{D1} = 100 - \ell.age \,||\, SOH_{D1} = 100 - o.km \tag{91}$$

$$SOH_{D2} = 100 - 0.001673.e^{(0.022.DOD + 0.4124)}.\left(1 - 0.0212.SOC_m\left(1 + \frac{SOC_m}{84}\right).FEC\right) \tag{92}$$

$$y(N) = a_1.e^{a_2.N} + a_3.e^{a_4.N} \tag{95}$$

A cell-to-package aging analysis for NMC-type SLB aging characteristics with uncertainties (faster or slower degradation behavior during $SOH_{initial}$ and second lifetime) was performed Seger et al.[112] The cycle depth, SOC, and current value are stress factors, and detailed parameterization is provided based on experimental and open-access data. σ was used to represent the exponential capacity loss for the effect of stress factors on aging. Moreover, the effect of cycle depth on the expected number of equivalent cycles is considered via Wöhler curves. These curves are obtainable from the battery manufacturers. γ is used to weight the possible SOC pairs. Finally, the derived and curve-fitted degradation function is as in Equation (96). The SOC is closely related to the C-rate, the uncertainties (ε_1 and ε_2), and the cumulative cycling capacity (Q_c). The degradation model in Equation (97)[113] for EV LFP type SLBs (BYD e5, BYD e6, and JAC iEV6) is derived from laboratory results by Yang et al.[114]

$$Q_{loss} = 0.019.e^{\left[\left(1.5365.10^{-4}.\left(SOC_m^{\%}\right)^2 - 1.5365.10^{-2}.SOC_m^{\%} + 0.3841 + \frac{\Delta SOC^{\%}}{100}\right)\right.} .\left(0.8277.e^{0.3904.|C_{rate}|}\right)\left.\right].0.009.\varepsilon_1.Q_c - \varepsilon_2 \tag{96}$$

$$C_k = \eta^k C_0 \tag{97}$$

The average performance for SLBs can also be estimated by the model predictive control (MPC) technique, considering the average curves of renewable energy production and power demand. If the SLB's SOH before commissioning is known, the number of cycles corresponding to the degradation curves can be

$$C_{SLB} = n.SOH_{EOL}^{C}.C_{SLB,0}.e^{-\left(\frac{1}{\Delta SOC}\int_{SOC_1}^{SOC_2} e^{\frac{34.6.SOC}{8.314}}.e^{\frac{131.36}{8.314}}.e^{-\frac{67.6}{8.314.T_{SLB}}}.131.36.SOC\right).\left(e^{\frac{I_{SLB}}{I_0}e^{\frac{49.45}{8.314.T_{SLB}}-24.06}}\right).t} \tag{93}$$

$$R_{SLB} = n.SOH_{EOL}^{R}.R_{SLB,0}.e^{\mathcal{B}.\left(\frac{1}{\Delta SOC}\int_{SOC_1}^{SOC_2} e^{\frac{29.2.SOC}{8.314}}.e^{\frac{111.24}{8.314}}.e^{-\frac{57.82}{8.314.T_{SLB}}}.111.24.SOC\right).\left(e^{\frac{I_{SLB}}{I_0}e^{\frac{49.45}{8.314.T_{SLB}}-24.06}}\right).t} \tag{94}$$

25784862, 2024, 4, Downloaded from https://onlinelibrary.wiley.com/doi/10.1002/est2.661 by Yildiz Technical University, Wiley Online Library on [13/06/2024]. See the Terms and Conditions (https://onlinelibrary.wiley.com/terms-and-conditions) on Wiley Online Library for rules of use; OA articles are governed by the applicable Creative Commons License

estimated. The updated SOH for the next day is calculated by Equation (98) based on the incremental cycle rule. The capacity loss of SLB during operation $\Delta Q = Q_{\text{rated}}.(\text{SOH}(24) - \text{SOH}(0))$.[115] The cycle step increment is determined based on the online SOH estimation by Cheng et al.[116] by dividing the accumulated charge/discharge energy in the SLB by the full charge-discharge cycle power over the SOH update timescale (168 h per week). This way, the $\text{cycle}_{k,j}(\tau+1)$, is updated. Therefore, the aging in the cumulative cycle makes it easier to estimate the SOH with Equations (99) and (100). The degradation model considering the DOD, charge and discharge current, and SLB temperature is explained in Equation (101). Such mathematical models are highly relevant for SOH estimation via long short-term memory (LSTM).[117] Actual values are represented by n and reference values by the reference.

$$\text{cycle}(t=24) = \frac{\sum_{t=0}^{23} |P_b(t)|}{2.Q_{\text{rated}}.\text{SOH}(0)} + \text{cycle}(t=0) \tag{98}$$

$$\text{SOH}_{k,j}^{p}(\tau) \sim \mathcal{KF}\left(\mu'_{k,j}(\tau), {\sigma'_{k,j}}^{2}(\tau)\right) \tag{99}$$

$$\text{cycle}_{k,j}(\tau+1) = \frac{\sum_{t=168\tau}^{168(\tau+1)} l\left(\text{SOH}_{k,j}^{p}(\tau), \text{SOH}_{k}^{p}(\tau), P_{k}^{ch}(\tau)\right) + l\left(\text{SOH}_{k,j}^{p}(\tau), \text{SOH}_{\text{k}}^{\text{p}}(\tau), P_{k}^{\text{dis}}(\tau)\right)}{2.Q_{k,j,\text{rated}}.\text{SOH}_{k,j}^{p}(\tau)} + \text{cycle}_{k,j}(\tau) \tag{100}$$

$$N_c(n) = N_{c,\text{ref}} \left(\frac{\text{DOD}(n)}{\text{DOD}_{\text{ref}}}\right)^{-\frac{1}{\xi}} . \left(\frac{I_{\text{dis}}(n)}{I_{\text{dis,ref}}}\right)^{-\frac{1}{Y_1}} . \left(\frac{I_{\text{chg}}(n)}{I_{\text{chg,ref}}}\right)^{-\frac{1}{Y_2}} . e^{\left[-\psi.\left(\frac{1}{T_{\text{ref}}} - \frac{1}{T_a(n)}\right)\right]} \tag{101}$$

8 | CONCLUSIONS

This review provides an overview of battery models and circuit equations commonly used by researchers. It also presents an outlook on the aging mechanism and estimation methods for health status. A comprehensive discussion of the proposed analytical and deterministic functions for extra operating costs due to battery aging and degradation is the main objective of the review. The shortcomings of analytical, deterministic, and innovative approaches are addressed, considering the stress factors affecting the aging mechanism and cost. Traditional and AI-based methods focusing on estimation methods are beyond the scope of the review. Researchers are focused on the Arrhenius equations because they can appropriately express temperature dependence. In addition to temperature and SOC, throughput is also considered in Arrhenius equations to determine calendar aging properly. The impact of factors such as C-rate, DOD, charge/discharge current, and throughput on cycle aging is a phenomenon that needs to be considered from many perspectives (different battery chemistries and experimental methods, various storage application areas, and different curve fitting and machine learning approaches). Therefore, a recognized aging function is still lacking regardless of battery chemistry. The effects of operational conditions on the aging phenomenon will vary due to the unpredictability of internal battery chemical reactions. Accordingly, the aging phenomenon should consider the increase in internal impedance rather than focusing on capacity reduction. Accelerated developments in aging can be followed by knowing the formation levels of LLI, LAM, and SEI. Another shortcoming is the need for hybrid consideration of specific application areas and internal chemical developments. Data storage and processing (blockchain) of battery aging and learning approaches for relevant battery chemistry can overcome the problems of deterministic methods. Using suitable data mining, novel or alternative battery technologies can be developed by learning from past mistakes. This review is expected to help many stakeholders and provide a roadmap for the unknown nature of battery aging. Moreover, deterministic aging functions can be easily applied to optimization problems, facilitating the task of researchers. Novel functional approaches based on neglected factors in aging are also discussed. Future work will focus on approaches for estimating remaining capacity and SOH in batteries and robustness performance. Innovative methods for aging predictions and uncertainty will be investigated to address the feasibility of future report projections. The variable cost's financial, environmental, and technical impact on hybrid renewable

25784862, 2024, 4, Downloaded from https://onlinelibrary.wiley.com/doi/10.1002/est2.661 by Yildiz Technical University, Wiley Online Library on [13/06/2024]. See the Terms and Conditions (https://onlinelibrary.wiley.com/terms-and-conditions) on Wiley Online Library for rules of use; OA articles are governed by the applicable Creative Commons License

systems caused by the unknown aging phenomenon will be detailed. Since each storage alternative has shortcomings for the desired system performance, a comprehensive review of hybrid energy storage will also be considered.

NOMENCLATURE

E_a	the activation energy (J mol^{-1})
z	the power law exponent
R	the gas constant
T	the absolute temperature (°C)
B,A	the pre-exponential factor
Ah	the throughput or dependence
C_{rate}	the speed at which a battery is fully charged or discharged
α,β	state of charge and C-rate dependence
η	models the current rate normalized to battery charge capacity dependence
SOC_{avg}	the mean state of charge over the time interval of cycling
SOC_{dev}	the deviation state of charge over the time interval of cycling
$k_1,...,k_4$	the experimental results' fitting
$k_5,...,k_{11}$	the least-square fitting coefficient
I_d	the constant discharge current
DOD	the depth of discharge (%)
I_{ch}	the fast charging current (A)
κ,ρ,λ	the experimental data fitting
V	the storage voltage (V)
$k_{12},...,k_{17}$	the experimental results' fitting
V_{avg}	the average storage voltage (V)
SOE	the state of energy (%)
$k_{18},...,k_{22}$	the fitting parameters from experiments
$Q_{\text{cal},0}$	the nominal capacity fade in the condition with SOE_0
$\beta_{\text{cal}}[n]$	the battery energy storage capacity fade
$\beta_{\text{cyc}}[n]$	the battery energy storage capacity loss due to cyclic aging
n	the discrete time step
$P_b[\tau]$	the battery charge or discharge power at any time step
E_b	the original battery capacity (kWh)
L_{cyc}	the battery full equivalent cycles
$I_{\text{discharge}}(t)$	the battery discharge current at any time step
C_n	the battery nominal capacity (Ah)
$C_{d,0}$	the initial normalized battery capacity
$C_{\text{corr}}(t)$	the loss of corrosion capacity at any time step
$C_{\text{deg}}(t)$	the degradation capacity losses at any time step
B_{cyc}	an exponential factor in $\text{Ah}^{1-\text{Zcyc}}$
γ, V_b	a coefficient to determine the acceleration in aging due to the current (J mol^{-1} A^{-1})
Z_{cyc}	a constant with a value close to 0.5
β_0,β_1,β_2	the curve-fitting coefficients that can be determined based on the battery type and the experimental data provided by the manufacturer
N_{cycle}	the battery cycle life
$\psi_d(x)$	the time adjustment function
t_h	hours
$CI_{\alpha,\text{cal}}$	the percentage of calendar capacity loss
η_{ch}	the battery charging efficiency (%)
η_{dis}	the battery discharging efficiency (%)
$P_{ch}(t)$	the battery charging power at any time step
$P_{\text{dis}}(t)$	the battery discharging power at any time step
Δt	the time step
m	the stored time in months
$L_{\text{cyc}}^{80\%}$	the cycle life from 100% to 80% battery capacity
$h_\epsilon(t)$	the regression model for battery capacity dependence on temperature
$h_\gamma(t),h_\zeta(t)$	the regression model for battery cycle life dependence on depth of discharge and temperature
d	the depth of discharge of Li-ion battery
q	the dependency of cycle aging on cumulative throughput
p_t^-,p_t^+	the battery charging/discharging curves constraints and variables
I_c	the daily average C-rate
P_i^-	the discharging sample data
P_k^+	the charging sample data
y_{tk}	the choice of charging sample data
x_{ti}	the choice of discharging sample data
C_1	the double layer capacitance
$z(t)$	internal battery impedance
R_2,C_2	used to capture battery diffusion effects
i_{R2}	current flowing through R2 in the second R-C branch
C_N	rated battery capacity
$v_1(t)$	voltage on the first R-C branch
$v_2(t)$	voltage on the second R-C branch
R_o	the ohmic resistance that represents charge/discharge energy losses
$v(t)$	battery voltage at any time
$\text{OCV}(t)$	the open circuit voltage at any time

25784862, 2024, 4, Downloaded from https://onlinelibrary.wiley.com/doi/10.1002/est2.661 by Yildiz Technical University, Wiley Online Library on [13/06/2024]. See the Terms and Conditions (https://onlinelibrary.wiley.com/terms-and-conditions) on Wiley Online Library for rules of use; OA articles are governed by the applicable Creative Commons License

C_S	battery surface heat capacity
T_S	battery surface temperature
T_{amb}	ambient temperature
T_C	battery internal temperature
R_u	heat convection resistance
R_C	heat conduction resistance
C_C	battery internal heat capacity
$I(t)$	battery charging current at any time
$V(t)$	battery terminal voltage
x	state vector
u	input vector
$f(x,u)$	nonlinear state equation of system
L	the nonlinear capacity fade of a new battery
σ,δ	Arrhenius coefficient
k_σ	SOC stress coefficient
k_T	calendar aging stress coefficient
$\overline{T}'$	total duration of T' in days
K	surrounding temperature, (K)
i^*	constant charge during T''(A h)
$\zeta,\varrho,\varsigma,\daleth,\varepsilon$	cycle aging coefficients, (kW^{-1} K^{-2}), (kW^{-1} K^{-1}), (kW^{-1}), (K^{-1} h), (h)
ϑ	calendar aging coefficient defining an Arrhenius factor ($months^{-1/2}$)
T'	subset of T indexed by t'
$Q^{T'}$	capacity loss of electric storage during T' (%)
$Z_W(t)$	the weighted number of cycles
C_N	the battery cell nominal capacity in Ah
$I_d(\tau)$	the battery discharging current
$c_{SOC,0}, c_{SOC,min}$	coefficient indicating the effect of SOC and discharge current on battery degradation process
$f_I(t)$	the current factor representing the effect of the discharged battery current
f_{strat}	stratification coefficient
$f_{acid}(\tau)$	the influence of the acid stratification on the weighted number of cycles
L_{EES}	calendar life of the battery storage
L_{float}	the float life of battery
N_d^{fail}	the maximum number of cycles to fail with 20% of capacity loss
$P^{\wedge}_{EES,k}$	the charging states of electrical energy storage
s_t	the grid control signal
η_{EES}	electrical energy storage efficiency
$P^{\vee}_{EES,k}$	the discharging states of electrical energy storage
$E_{EES,rated}$	electrical energy storage rated capacity
W	the number of operation days
C_k	the reversible or remaining capacity at cycle k
η^k	the battery degradation rate
C_0	the initial capacity of the battery
ℓ	the parameter that relates the aging of the battery with the time
$\mathscr{o}$	coefficient relating battery size-dependent state of health to mileage
FEC	full equivalent cycles
F	The Faraday constant
Q_e	the pre-exponential factor
$\mathcal{M}$	the electrode transfer coefficient
$\hbar$	the decay rate
$N_c(n)$	the cycle life for the actual values
$N_{c,ref}$	the cycle life at reference values
ξ, Y_1, Y_2, ψ	stress exponents
K_f	rate constant
a,b	the parameters related to the internal impedance
c,d	the aging rate
k	the cycle number
cd	cycle depth
nc	number of cycles
P_{fade}	the battery cycling power fade
C_{fade}	the battery cycling capacity fade
$\mathcal{y}_1$	a starting offset
$\mathcal{y}_2$	the factor by which the exponential curve scales the changing cycle DOD in each cycle
C_k	the capacity at the kth cycle
f	the linear cycle and calendar aging
EOL	battery end of life
I_{SLB}	second-life battery current
I_0	a current amplitude scaling factor equal to 2.83
$\alpha_{cap}, \alpha_{res}$	the aging rate during a test of time t
β_{cap}, β_{res}	the dependency of cycle aging factor
Q	the charge throughput
ØV	quadratic average voltage dependency
$c(t)$	battery aging cost for time t
$\mathrm{sgn}[g_t(t)]$	the sign function with respect to output power gt at time t
$g_t(t)$	output power at time t
$\Phi(\delta)$	the incremental aging resulting from the discharge depth δ
E	the rated energy capacity of the battery
L	the total life expectation of batteries
δ	the discharge depth
R	replacement cost of batteries
$c_u(t)$	unscheduled interchange cost for time t
$p(f)$	the unscheduled interchange price concerning system frequency
$\Delta P(t)$	the real-time power imbalance

25784862, 2024, 4, Downloaded from https://onlinelibrary.wiley.com/doi/10.1002/est2.661 by Yildiz Technical University, Wiley Online Library on [13/06/2024]. See the Terms and Conditions (https://onlinelibrary.wiley.com/terms-and-conditions) on Wiley Online Library for rules of use; OA articles are governed by the applicable Creative Commons License

$\alpha_1, \alpha_2, \alpha_3$	predefined constants
β_2, β_3	predefined coefficients
f_0	the base frequency
$P_X(t)$	charge/discharge power at time t
N_X^{parallel}	amount of cells in parallel in BES
N_X^{series}	amount of cells in series in BES
$i_X^{\text{cell}}(t)$	current rate at time t
$\Delta E_X^{\text{cycle}}(t)$	cyclic aging at time t
$\Delta E_X^{\text{cal}}(t)$	calendar ageing at time t
$\Delta E_X^{\text{tot}}(t)$	the capacity lost per time step
$E_{\text{BES}}^{\max}$	initial maximum BES capacity
$u(T,t)$	the degradation function of the battery under temperature stress
$\mathrm{u}(R_d,t)$	the degradation function of battery modules at different discharge rates
$\mathrm{u}(T,R_d)$	capacity degradation under compound stress
R_d	discharge rate
$K_{t+i}(T_{t+i},R_{d,t+i})$	the degradation coefficient function for the dynamic conditions
Q_c	the cumulative cycled capacity of the cell
ε_1	parameters used to model the uncertainties. Normal law with $\mu = 1; \text{SD} = 0.1$
ε_2	parameters used to model the uncertainties. Normal law with $\mu = 0.019; \text{SD} = 0.0358$
δ	the film thickness is composed of lithium products
i_k	the rate (current) of the side reaction
M, L, α, ρ, F	all constant for a given reaction and a given battery
r_f	the film resistance
η_c	the concentration variations near the surface of the electrode
β	a degradation fitting parameter was used to capture the cycle depth effect (DOD) and the average voltage (V_{mean}).
s	the number of days
I_b	the battery current (charging and discharging)
$d0_{T_{(t)}}$	the battery temperature dependency based on the Arrhenius formula for all the mechanisms
$b_0, ..., b_3$	coefficients reflecting the growth of the SEI layer over time and mechanical fracture at decreasing battery cycle
N_c	the number of equivalent full cycles
c_1	coefficient used for mechanical stress due to expansion and contraction of electrode materials during charging/discharging
d_3	the coefficient by which the Ah throughput in the first few cycles causes the temperature to increase
Q_{SEI}	capacity fade due to solid electrolyte interphase layer
Q_{AM}	the battery active material loss
Q_{pos}	the positive electrode storing capability
E_{bat}	the energy stored inside the battery
$\text{Cost}_{\text{deg}}^t$	the battery degradation cost
Cost_{bat}	the battery module cost (€/kW)
$\text{Cycle}_{\text{rep}}$	related cycles-to-failure
η_{conv}	the converter efficiency (%)
$C_{\text{O\&M}}(t)$	the operating cost during battery discharging
C_{inv}^b	investment cost of battery
$C_{\text{O\&M}}^b$	battery operation and maintenance costs
dr, r	discount rate
RV	residual value of Li-ion battery
X_T^{Ξ}	temperature dependent battery capacity factor
X_T^{γ}	temperature dependent battery cycle-life factor
X_d^{γ}	depth of discharge dependent battery cyclelife factor
γ_{ref}	reference cycle life of Li-ion battery
Ξ_{ref}	rated energy capacity of Li-ion battery
C^b	battery degradation costs
B_1, B_2	cycle aging coefficients
$\mathcal{H}$	set of time steps (simulation horizon)
p_t^-/p_t^+	output/input power from/to the battery cells
$C^{b,0}$	purchase cost of battery ($)
C_E	the one-cycle degradation cost
X_t^s	the binary indicator for the SoC segment
si	the segment index
N_{seg}	a total number of segments
$Q_{\max}$	the battery nominal energy (kWh)
g_n	the battery DOD within an allowable range (%)
f_n	the number of cycles to failure under g_n
$P_{\text{ESS}}(t)$	the average output power during the time interval
N_{cd}	the total number of charging/discharging cycles
k_p	Peukert lifetime constant is restricted between 1.1 and 1.3

25784862, 2024, 4, Downloaded from https://onlinelibrary.wiley.com/doi/10.1002/est2.661 by Yildiz Technical University, Wiley Online Library on [13/06/2024]. See the Terms and Conditions (https://onlinelibrary.wiley.com/terms-and-conditions) on Wiley Online Library for rules of use; OA articles are governed by the applicable Creative Commons License

C_R	the rated battery capacity under the rated current rate
D_R	the rated DOD measures the rated battery life
L_R	the number of cycles to failure under the rated discharge C-rate and D_R
D_A	the actual DOD under the actual condition
D_R	the real DOD under the real condition
u_0, u_1	best-fit parameters of battery cycle life vs DOD curve
C_R	the battery capacity under the real condition
C_A	the battery capacity under the actual condition
d_{actual}	the actual ampere-hour discharge value
$I_{\text{ESS}}(t)$	the energy storage system current at any time
$\lambda_1, \lambda_2, \lambda_3$	coefficients that minimize the total error between the experiment data and the CAPN model
$Q_{\text{loss}}^{\text{Linear}}(T)$	the accumulated capacity loss for the linear model
$Q_{\text{loss}}^{\text{PLET}}(T)$	the accumulated capacity loss for a DOD-based Peukert lifetime energy throughput
$Q_{\text{loss}}^{\text{NREL}}(T)$	the accumulated capacity loss for National Renewable Energy Laboratory model
$Q_{\text{loss}}^{\text{Arrhenius}}(T)$	the accumulated capacity loss for Arrhenius model
$Q_{\text{loss}}^{\text{CAPN}}(T)$	the accumulated capacity loss for the C-rate combined Arrhenius-PLET-NREL model
i_{R1}	current flowing through R1 in the first R-C branch
R_1	the charge transfer resistance
$SOH_{k,j}^{p}(\tau)$	a function of its cells' SoH, which is affected by the topology of the cell connection
$\mathcal{KF}$	the short-term estimation probability density function (PDF) and the long-term prediction model PDF
$\mu'_{k,j}$	the combined mean of the estimation
$\sigma'_{k,j}$	the combined variance of the estimation
k	the k th battery pack
j	the j th battery cell
$Q_{k,j,\text{rated}}$	the rated battery capacity
$cycle_{k,j}(\tau+1)$	the accumulated number of cycles
$P_b(t)$	the second-life battery power output
Q_{rated}	the second-life battery original capacity
$\text{SOH}(0)$	the state of health at the beginning of the day
ΔQ	the capacity degradation
tcc_e	total capital cost (energy)
cap_e	energy capacity
P_{esc}	charging cost escalator
cap_p	power capacity
t_c	construction time
EPR	energy to power ratio
a_{deg}	annual battery capacity degradation
η_{rt}	the battery round-trip efficiency
TDC_{FB}	total discounted cost for fresh battery
TDC_{SLB}	total discounted cost for second-life battery
rc_e	battery module repurposing cost
nmc	new battery module market cost
P_{el}	charging cost
o_{deg}	additional parameter to estimate the discounted energy to account for a battery replacement in the second-life system
rl_e	battery module replacement labor cost
t_r	replacement interval
$\text{O\&M}_p$	fixed O&M cost (power)
N	the current cycle number
h	index for a time interval
Q_h^{cal}	the lithium-ion battery calendar aging
SOC_h	state of charge at time interval
E_h^{BES}	battery energy rating at time interval
Ω^h	set of time intervals
C_{cap}	the maximum ability of the new battery to store the current
R_i	internal resistance of the cell
C_{cal}	the heat capacity of the calorimeter
C_{cell}	the cell capacity
$I_{\text{sm}}(t)$	a small alternating current (AC) that produces a small AC voltage $U(t)$ response to the battery
$Z(1)_{\text{adj}}$	the adjusted impedance to 25°C
$Z(1)_{\text{model}}$	the 1 Hz impedance model
T_{cell}	cell temperature model
Q_P	the total charge capacity available from the positive electrode
$T_{\text{CC+CV}}$	battery temperature after a complete constant current and constant voltage (CC-CV) charging for any cycle
ε_p	volume fraction of a phase
σ_p	conductivity of electrode (S/m)
ϕ_1	the solid phase potentials between the positive and negative ends of the Li-ion cell sandwich
L_P	length of the cell (positive electrode) (m)

25784862, 2024, 4, Downloaded from https://onlinelibrary.wiley.com/doi/10.1002/est2.661 by Yildiz Technical University, Wiley Online Library on [13/06/2024]. See the Terms and Conditions (https://onlinelibrary.wiley.com/terms-and-conditions) on Wiley Online Library for rules of use; OA articles are governed by the applicable Creative Commons License

$0t$	initial time (s)
L_n	length of the cell (negative electrode) (m)
J_s	side reaction current densities
θ_1	the SOC of the electrode
$Q_{\max}$	the initial rated capacity of the cell
$\mathcal{B}$	a scaling factor for the resistance as a function of the state of charge
$\mathrm{SOH}_{\mathrm{EOL}}^{\mathrm{C}}$	end of life state of health for capacity
$\mathrm{SOH}_{\mathrm{EOL}}^{\mathrm{R}}$	end of life state of health for internal resistance
$y(N)$	the capacity fade of second-life battery
$a_1,...,a_4$	parameters to be determined through optimization tools.
R_{SLB}	the internal resistance of second-life battery pack
$R_{\mathrm{SLB},0}$	the initial internal resistance of the second-life battery
$C_{\mathrm{SLB},0}$	the nominal capacity of the second-life battery
C_{SLB}	the second-life battery pack capacity
T_{SLB}	second-life battery pack temperature
e	exponential
CTF	the cycles to failure profile
$f_{\mathrm{CTF}}(\mathrm{DOD})$	Gaussian function capturing correlation with battery DODs for CTF profile continuity
$f_{\mathrm{CC}}(\mathrm{Crate})$	the relationship between the capacity retention and the Crate
CTF_E	the equivalent battery cycles
$\eta(k)$	the equivalent battery aging factor
k	the index of the extracted battery cycles
TBA	the aging index for the cloud battery modeling process
$\Delta\mathrm{SOH}_k$	the drop of state of health under multiple stresses
$F(\mathrm{Crate})$	pre-exponential factor
$\mathscr{r}$	controls the vertical scaling of the degradation rate
ƒ	primarily controls the horizontal scaling and peak position of the degradation rate.
$\mathscr{k}$	battery charge cycle
$\mathscr{v}_p$	the process noise
x_k, x_{k-1}	step-by-step degradation
$k_{\mathrm{Cal}}(T,\mathrm{SOC})$	the stress factor due to calendar aging effects, as a function of temperature and storage SOC
$k_{\mathrm{Cyc,High}\ T}(T)$	the current rate dependence for the high-temperature mechanism
$k_{\mathrm{Cyc,Low}\ T}(T,I_{ch})$	the current rate dependence for the low-temperature mechanism
R_g	the universal gas constant
α, k_0	fitting parameters
$U_{a,\mathrm{Ref}}$	the anode open circuit potential (ref)
$U_a(\mathrm{SOC})$	the anode open circuit potential, SOC dependent
$E_{a,\mathrm{Cal}}$	the calendar activation energy
$E_{a,\mathrm{Cyc,Low}\ T}$	the cycle activation energy for the low-temperature
C_0	nominal cell capacity
τ, φ	the integration variables
κ_D	the linearized cyclic aging rate corresponding to unit cycle depth
η_c, η_d	charging and discharging efficiencies of battery energy storage system
P^{ec}, P^{ed}	charging and discharging power for battery (Pec ≥ 0, Ped ≥ 0)
$E_{\max}$	the maximum rated energy capacity
κ_{cal}	linearized calendar aging rate corresponding to unit operation time
L^{com}	comprehensive linearized aging rate
P_{rated}	rated charging-discharging power
κ_1^D	cyclic aging rate corresponding to unit cycle depth at life stage 1
$a_{m_{p,l}}, b_{m_{p,l}}$	parameters in piecewise linear calculation function for cyclic accelerating factor due to the charging-discharging rate at segment m_ρ and life stage l
χ_1	calendar accelerating factor at life stage l
κ_1^{cal}	calendar aging rate corresponding to unit operation time at life stage 1
$L_l^{\mathrm{com},m}$	comprehensive multistage aging rate at life stage l
ζ	cell capacity or internal resistance at nominal conditions (Ah or Ohm)
t^α	a time-dependent factor
$k_{\mathrm{SEI}}, k_{\mathrm{LAM}}, \lambda$	fitting pseudo-physical parameter
$j_n(t)$	current density (Am^{-2})
θ	the variation in overpotential
$y_1,...,y_6, I_0$	the calibration of the model
I	the applied current
μ, SD	mean, SD
T'	some cycle temperature
$P(T')$	the probability that the temperature T'
$b_1(i,T), b_2(i,T)$	functions of discharge rate and temperature
c	the charge capacity

AUTHOR CONTRIBUTIONS

Musa Terkes: conceptualization; visualization; writing-original draft; methodology. **Alpaslan Demirci**: supervision; validation; investigation; writing–review and editing. **Erdin Gokalp**: supervision; validation; investigation.

25784862, 2024, 4, Downloaded from https://onlinelibrary.wiley.com/doi/10.1002/est2.661 by Yildiz Technical University, Wiley Online Library on [13/06/2024]. See the Terms and Conditions (https://onlinelibrary.wiley.com/terms-and-conditions) on Wiley Online Library for rules of use; OA articles are governed by the applicable Creative Commons License

ACKNOWLEDGMENTS

Analyzes and comments made in this document belong to the authors. Any institution, company, etc., does not support the article.

FUNDING INFORMATION

Authors have no financial or non-financial interests that are directly or indirectly related to the work submitted for publication.

CONFLICT OF INTEREST STATEMENT

The authors declare that they have no known competing financial interests or personal relationships that could have appeared to influence the work reported in this article.

DATA AVAILABILITY STATEMENT

Data sharing not applicable to this article as no datasets were generated or analysed during the current study.

ORCID

Alpaslan Demirci https://orcid.org/0000-0002-1038-7224

REFERENCES

1. Wang S, Jin S, Bai D, Fan Y, Shi H, Fernandez C. A critical review of improved deep learning methods for the remaining useful life prediction of lithium-ion batteries. *Energy Rep*. 2021;7:5562-5574. doi:10.1016/j.egyr.2021.08.182
2. Eckhouse B. *The Battery Boom Will Draw 620 Billion Dollar in Investment by 2040*. BloombergNEF; 2018. Accessed April 10, 2024. https://www.bloomberg.com/news/articles/2018-11-06/the-battery-boom-will-draw-1-2-trillion-in-investment-by-2040
3. Engel H, Hertzke P, Siccardo G. Second-life EV batteries: The newest value pool in energy storage. McKinsey & Company; 2019. Accessed April 11, 2024. https://www.mckinsey.com/industries/automotive-and-assembly/our-insights/second-life-ev-batteries-the-newest-value-pool-in-energy-storage
4. Guidehouse INSIGHTS. *Second Life Battery Market*. Guidehouse Inc; 2020. Accessed April 12, 2024. https://guidehouseinsights.com/reports/second-life-battery-markets
5. The International Energy Agency. *Net Zero by 2050: A Roadmap for the Global Energy Sector*. IEA; 2021:1-224. Accessed April 15, 2024. https://www.iea.org/reports/net-zero-by-2050
6. Zu C-X, Li H. Thermodynamic analysis on energy densities of batteries. *Energ Environ Sci*. 2011;4(8):2614. doi:10.1039/c0ee00777c
7. Deshwal D, Sangwan P, Dahiya N. Economic analysis of lithium ion battery recycling in India. *Wirel Pers Commun*. 2022;124:3263-3286. doi:10.1007/s11277-022-09512-5
8. Meshram P, Pandey BD, Mankhand TR. Extraction of lithium from primary and secondary sources by pre-treatment, leaching and separation: a comprehensive review. *Hydrometallurgy*. 2014;150:192-208. doi:10.1016/j.hydromet.2014.10.012
9. Amit K. The spiralling environmental cost of our lithium battery addiction. *Wired*. 2018;9:1-15.
10. Davidsson Kurland S. Energy use for gwh-scale lithium-ion battery production. *Environ Res Commun*. 2020;2(1):012001. doi:10.1088/2515-7620/ab5e1e
11. Gailani A, Al-Greer M, Short M, Crosbie T. Degradation cost analysis of Li-ion batteries in the capacity market with different degradation models. *Electronics*. 2020;9(1):90. doi:10.3390/electronics9010090
12. Lai X, Zheng Y, Sun T. A comparative study of different equivalent circuit models for estimating state-of-charge of lithium-ion batteries. *Electrochim Acta*. 2018;259:566-577. doi:10.1016/j.electacta.2017.10.153
13. Xu Y, Hu M, Fu C, Cao K, Su Z, Yang Z. State of charge estimation for lithium-ion batteries based on temperature-dependent second-order RC model. *Electronics*. 2019;8(9):1012. doi:10.3390/electronics8091012
14. Zhang C, Li K, Deng J, Song S. Improved Realtime state-of-charge estimation of LiFePO battery based on a novel thermoelectric model. *IEEE Trans Ind Electron*. 2017;64(1):654-663. doi:10.1109/TIE.2016.2610398
15. Liu K, Hu X, Yang Z, Xie Y, Feng S. Lithium-ion battery charging management considering economic costs of electrical energy loss and battery degradation. *Energ Conver Manage*. 2019;195:167-179. doi:10.1016/j.enconman.2019.04.065
16. Gould CR, Bingham CM, Stone DA, Bentley P. New battery model and state-of-health determination through subspace parameter estimation and state-observer techniques. *IEEE Trans Veh Technol*. 2009;58(8):3905-3916. doi:10.1109/TVT.2009.2028348
17. Chiasson J, Vairamohan B. Estimating the state of charge of a battery. *IEEE Trans Control Syst Technol*. 2005;13(3):465-470. doi:10.1109/TCST.2004.839571
18. Chaoui H, Sicard P, Ndjana HJN. Adaptive state of charge (SOC) estimation for batteries with parametric uncertainties. *2010 IEEE/ASME International Conference on Advanced Intelligent Mechatronics*, Montreal, QC, Canada; 2010:703-707. doi:10.1109/AIM.2010.5695870
19. Vasebi A, Bathaee SMT, Partovibakhsh M. Predicting state of charge of lead-acid batteries for hybrid electric vehicles by extended Kalman filter. *Energ Conver Manage*. 2008;49(1):75-82. doi:10.1016/j.enconman.2007.05.017
20. Vasebi A, Partovibakhsh M, Bathaee SMT. A novel combined battery model for state-of-charge estimation in lead-acid batteries based on extended Kalman filter for hybrid electric vehicle applications. *J Power Sources*. 2007;174(1):30-40. doi:10.1016/j.jpowsour.2007.04.011
21. Kim I-S. Nonlinear state of charge estimator for hybrid electric vehicle battery. *IEEE Trans Power Electron*. 2008;23(4):2027-2034. doi:10.1109/TPEL.2008.924629
22. Bhangu BS, Bentley P, Stone DA, Bingham CM. Nonlinear observers for predicting state-of-charge and state-of-health of Lead-acid batteries for hybrid-electric vehicles. *IEEE Trans Veh Technol*. 2005;54(3):783-794. doi:10.1109/TVT.2004.842461
23. Babazadeh R, Khiabani AG. *Nonlinear observer design for RC battery model for estimating state of charge and State of Health Based on State-Dependent Riccati Equation. 2018 IEEE Electrical Power and Energy Conference (EPEC)*, Toronto, ON, Canada; 2018:1-5. doi:10.1109/EPEC.2018.8598459
24. Ruetschi P. Aging mechanisms and service life of lead–acid batteries. *J Power Sources*. 2004;127(1–2):33-44. doi:10.1016/j.jpowsour.2003.09.052

25784862, 2024, 4, Downloaded from https://onlinelibrary.wiley.com/doi/10.1002/est2.661 by Yildiz Technical University, Wiley Online Library on [13/06/2024]. See the Terms and Conditions (https://onlinelibrary.wiley.com/terms-and-conditions) on Wiley Online Library for rules of use; OA articles are governed by the applicable Creative Commons License

25. Birkl CR, Roberts MR, McTurk E, Bruce PG, Howey DA. Degradation diagnostics for lithium ion cells. *J Power Sources*. 2017;341:373-386. doi:10.1016/j.jpowsour.2016.12.011
26. Xiong R, Pan Y, Shen W, Li H, Sun F. Lithium-ion battery aging mechanisms and diagnosis method for automotive applications: recent advances and perspectives. *Renew Sustain Energy Rev*. 2020;131:110048. doi:10.1016/j.rser.2020.110048
27. Che Y, Hu X, Lin X, Guo J, Teodorescu R. Health prognostics for lithium-ion batteries: mechanisms, methods, and prospects. *Energ Environ Sci*. 2023;16(2):338-371. doi:10.1039/D2EE03019E
28. Maheshwari A, Paterakis NG, Santarelli M, Gibescu M. Optimizing the operation of energy storage using a non-linear lithium-ion battery degradation model. *Appl Energy*. 2020;261:114360. doi:10.1016/j.apenergy.2019.114360
29. Zia MF, Elbouchikhi E, Benbouzid M. Optimal operational planning of scalable DC microgrid with demand response, islanding, and battery degradation cost considerations. *Appl Energy*. 2019;237:695-707. doi:10.1016/j.apenergy.2019.01.040
30. Lam L, Bauer P. Practical capacity fading model for Li-ion battery cells in electric vehicles. *IEEE Trans Power Electron*. 2013;28(12):5910-5918. doi:10.1109/TPEL.2012.2235083
31. Cordoba-Arenas A, Onori S, Guezennec Y, Rizzoni G. Capacity and power fade cycle-life model for plug-in hybrid electric vehicle lithium-ion battery cells containing blended spinel and layered-oxide positive electrodes. *J Power Sources*. 2015;278:473-483. doi:10.1016/j.jpowsour.2014.12.047
32. Hesse HC, Martins R, Musilek P, Naumann M, Truong CN, Jossen A. Economic optimization of component sizing for residential battery storage systems. *Energies*. 2017;10(7):835-853. doi:10.3390/en10070835
33. Nuroldayeva G, Serik Y, Adair D, Uzakbaiuly B, Bakenov Z. State of health estimation methods for lithium-ion batteries. *Int J Energy Res*. 2023;2023:1-21. doi:10.1155/2023/4297545
34. Chen L, Lü Z, Lin W, Li J, Pan H. A new state-of-health estimation method for lithium-ion batteries through the intrinsic relationship between ohmic internal resistance and capacity. *Measurement*. 2018;116:586-595. doi:10.1016/j.measurement.2017.11.016
35. Choi W, Shin H-C, Kim JM, Choi J-Y, Yoon W-S. Modeling and applications of electrochemical impedance spectroscopy (EIS) for Lithium-ion batteries. *J Electrochem Sci Technol*. 2020;11(1):1-13. doi:10.33961/jecst.2019.00528
36. Fernández Pulido Y, Blanco C, Anseán D, García VM, Ferrero F, Valledor M. Determination of suitable parameters for battery analysis by electrochemical impedance spectroscopy. *Measurement*. 2017;106:1-11. doi:10.1016/j.measurement.2017.04.022
37. Choi S, Wang G. Advanced lithium-ion batteries for practical applications: technology, development, and future perspectives. *Adv Mater Technol*. 2018;3(9):1700376-1700396. doi:10.1002/admt.201700376
38. Wei X, Zhu B, Xu W. *Internal resistance identification in vehicle power lithium-ion battery and application in lifetime evaluation. 2009 International Conference on Measuring Technology and Mechatronics Automation*, Zhangjiajie, China; 2009:388-392. doi:10.1109/ICMTMA.2009.468
39. Schweiger H-G, Obeidi O, Komesker O, et al. Comparison of several methods for determining the internal resistance of lithium ion cells. *Sensors*. 2010;10(6):5604-5625. doi:10.3390/s100605604
40. Kim J, Kowal J. Development of a Matlab/Simulink model for monitoring cell state-of-health and state-of-charge via impedance of lithium-ion battery cells. *Batteries*. 2022;8(2):8. doi:10.3390/batteries8020008
41. Kim J, Kowal J. A method for monitoring state-of-charge of lithium-ion cells using multi-sine signal excitation. *Batteries*. 2021;7(4):76. doi:10.3390/batteries7040076
42. Grolleau S, Delaille A, Gualous H, et al. Calendar aging of commercial graphite/LiFePO4 cell – predicting capacity fade under time dependent storage conditions. *J Power Sources*. 2014;255:450-458. doi:10.1016/j.jpowsour.2013.11.098
43. Wang S, Guo D, Han X, et al. Impact of battery degradation models on energy management of a grid-connected DC microgrid. *Energy*. 2020;207:118228. doi:10.1016/j.energy.2020.118228
44. Jafari M, Khan K, Gauchia L. Deterministic models of Li-ion battery aging: it is a matter of scale. *J. Energy Storage*. 2018;20:67-77. doi:10.1016/j.est.2018.09.002
45. Bloom I, Cole BW, Sohn JJ, et al. An accelerated calendar and cycle life study of Li-ion cells. *J Power Sources*. 2001;101(2):238-247. doi:10.1016/S0378-7753(01)00783-2
46. Wang J, Liu P, Hicks-Garner J, et al. Cycle-life model for graphite-LiFePO4 cells. *J Power Sources*. 2011;196(8):3942-3948. doi:10.1016/j.jpowsour.2010.11.134
47. Suri G, Onori S. A control-oriented cycle-life model for hybrid electric vehicle lithium-ion batteries. *Energy*. 2016;96:644-653. doi:10.1016/j.energy.2015.11.075
48. Han X, Ouyang M, Lu L, Li J. A comparative study of commercial lithium ion battery cycle life in electric vehicle: capacity loss estimation. *J Power Sources*. 2014;268:658-669. doi:10.1016/j.jpowsour.2014.06.111
49. Omar N, Monem MA, Firouz Y, et al. Lithium iron phosphate based battery–assessment of the aging parameters and development of cycle life model. *Appl Energy*. 2014;113:1575-1585. doi:10.1016/j.apenergy.2013.09.003
50. Wei Z, Quan Z, Wu J, Li Y, Pou J, Zhong H. Deep deterministic policy gradient-DRL enabled Multiphysics-constrained fast charging of lithium-ion battery. *IEEE Trans Ind Electron*. 2022;69(3):2588-2598. doi:10.1109/TIE.2021.3070514
51. Li Y, Vilathgamuwa M, Choi SS, et al. Design of minimum cost degradation-conscious lithium-ion battery energy storage system to achieve renewable power dispatchability. *Appl Energy*. 2020;260:114282. doi:10.1016/j.apenergy.2019.114282
52. Wang J, Kang L, Liu Y. Optimal scheduling for electric bus fleets based on dynamic programming approach by considering battery capacity fade. *Renew Sustain Energy Rev*. 2020;130:109978. doi:10.1016/j.rser.2020.109978
53. Ecker M, Gerschler JB, Vogel J, et al. Development of a lifetime prediction model for lithium-ion batteries based on extended accelerated aging test data. *J Power Sources*. 2012;215:248-257. doi:10.1016/j.jpowsour.2012.05.012
54. Bohlen O, Kowal J, Sauer DU. Ageing behaviour of electrochemical double layer capacitors. *J Power Sources*. 2007;173(1):626-632. doi:10.1016/j.jpowsour.2007.07.059
55. Bohlen O, Kowal J, Sauer DU. Ageing behaviour of electrochemical double layer capacitors. *J Power Sources*. 2007;172(1):468-475. doi:10.1016/j.jpowsour.2007.07.021
56. Waag W, Käbitz S, Sauer DU. Experimental investigation of the lithium-ion battery impedance characteristic at various conditions and aging states and its influence on the application. *Appl Energy*. 2013;102:885-897. doi:10.1016/j.apenergy.2012.09.030

25784862, 2024, 4, Downloaded from https://onlinelibrary.wiley.com/doi/10.1002/est2.661 by Yildiz Technical University, Wiley Online Library on [13/06/2024]. See the Terms and Conditions (https://onlinelibrary.wiley.com/terms-and-conditions) on Wiley Online Library for rules of use; OA articles are governed by the applicable Creative Commons License

57. Marongiu A, Roscher M, Sauer DU. Influence of the vehicle-to-grid strategy on the aging behavior of lithium battery electric vehicles. *Appl Energy*. 2015;137:899-912. doi:10.1016/j.apenergy.2014.06.063
58. Schmalstieg J, Käbitz S, Ecker M, Sauer DU. A holistic aging model for Li(NiMnCo)O2 based 18650 lithium-ion batteries. *J Power Sources*. 2014;257:325-334. doi:10.1016/j.jpowsour.2014.02.012
59. Sarasketa-Zabala E, Martinez-Laserna E, Berecibar M, Gandiaga I, Rodriguez-Martinez LM, Villarreal I. Realistic lifetime prediction approach for Li-ion batteries. *Appl Energy*. 2016;162:839-852. doi:10.1016/j.apenergy.2015.10.115
60. Sarasketa-Zabala E, Gandiaga I, Martinez-Laserna E, Rodriguez-Martinez LM, Villarreal I. Cycle ageing analysis of a LiFePO4/graphite cell with dynamic model validations: towards realistic lifetime predictions. *J Power Sources*. 2015;275:573-587. doi:10.1016/j.jpowsour.2014.10.153
61. Guenther C, Schott B, Hennings W, Waldowski P, Danzer MA. Model-based investigation of electric vehicle battery aging by means of vehicle-to-grid scenario simulations. *J Power Sources*. 2013;239:604-610. doi:10.1016/j.jpowsour.2013.02.041
62. Antoniadou-Plytaria K, Steen D, Tuan LA, Carlson O, Fotouhi Ghazvini MA. Market-based energy management model of a building microgrid considering battery degradation. *IEEE Trans Smart Grid*. 2021;12(2):1794-1804. doi:10.1109/TSG.2020.3037120
63. Mulleriyawage UGK, Shen WX. Optimally sizing of battery energy storage capacity by operational optimization of residential PV-battery systems: an Australian household case study. *Renew Energy*. 2020;160:852-864. doi:10.1016/j.renene.2020.07.022
64. Amini M, Nazari MH, Hosseinian SH. Optimal scheduling and cost-benefit analysis of lithium-ion batteries based on battery state of health. *IEEE Access*. 2023;11:1359-1371. doi:10.1109/ACCESS.2022.3232282
65. García-Vera Y, Dufo-López R, Bernal-Agustín J. Optimization of isolated hybrid microgrids with renewable energy based on different battery models and technologies. *Energies*. 2020;13(3):581. doi:10.3390/en13030581
66. Lee J-O, Kim Y-S. Novel battery degradation cost formulation for optimal scheduling of battery energy storage systems. *Int J Electr Power Energy Syst*. 2022;137:107795. doi:10.1016/j.ijepes.2021.107795
67. Yang F, Xie Y, Deng Y, Yuan C. Predictive modeling of battery degradation and greenhouse gas emissions from U.S. state-level electric vehicle operation. *Nat Commun*. 2018;9(1):2429. doi:10.1038/s41467-018-04826-0
68. Schiffer J, Sauer DU, Bindner H, Cronin T, Lundsager P, Kaiser R. Model prediction for ranking lead-acid batteries according to expected lifetime in renewable energy systems and autonomous power-supply systems. *J Power Sources*. 2007;168(1):66-78. doi:10.1016/j.jpowsour.2006.11.092
69. Petit M, Prada E, Sauvant-Moynot V. Development of an empirical aging model for Li-ion batteries and application to assess the impact of vehicle-to-grid strategies on battery lifetime. *Appl Energy*. 2016;172:398-407. doi:10.1016/j.apenergy.2016.03.119
70. Groot J, Swierczynski M, Stan AI, Kær SK. On the complex ageing characteristics of high-power LiFePO4/graphite battery cells cycled with high charge and discharge currents. *J Power Sources*. 2015;286:475-487. doi:10.1016/j.jpowsour.2015.04.001
71. Cardoso G, Brouhard T, DeForest N, Wang D, Heleno M, Kotzur L. Battery aging in multi-energy microgrid design using mixed integer linear programming. *Appl Energy*. 2018;231:1059-1069. doi:10.1016/j.apenergy.2018.09.185
72. Wu Y, Liu Z, Liu J, Xiao H, Liu R, Zhang L. Optimal battery capacity of grid-connected PV-battery systems considering battery degradation. *Renew Energy*. 2022;181:10-23. doi:10.1016/j.renene.2021.09.036
73. Topan PA, Ramadan MN, Fathoni G, Cahyadi AI, Wahyunggoro O. *State of charge (SOC) and state of health (SOH) estimation on lithium polymer battery via Kalman filter. Paper presented at 2016 2nd International Conference on Science and Technology-Computer (ICST)*. Yogyakarta, Indonesia: IEEE; 2016:93-96. doi:10.1109/ICSTC.2016.7877354
74. Hu X, Li SE, Jia Z, Egardt B. Enhanced sample entropy-based health management of Li-ion battery for electrified vehicles. *Energy*. 2014;64:953-960. doi:10.1016/j.energy.2013.11.061
75. Mathews I, Xu B, He W, Barreto V, Buonassisi T, Peters IM. Technoeconomic model of second-life batteries for utility-scale solar considering calendar and cycle aging. *Appl Energy*. 2020;269:115127. doi:10.1016/j.apenergy.2020.115127
76. Vermeer W, Chandra Mouli GR, Bauer P. Real-time building smart charging system based on PV forecast and Li-ion battery degradation. *Energies*. 2020;13(13):3415. doi:10.3390/en13133415
77. Fan F, Xu Y, Zhang R, Wan T. Whole-lifetime coordinated service strategy for battery energy storage system considering multi-stage battery aging characteristics. *J Mod Power Syst Clean Energy*. 2022;10(3):689-699. doi:10.35833/MPCE.2021.000034
78. Russell MB, King EM, Parrish CA, Wang P. Stochastic modeling for tracking and prediction of gradual and transient battery performance degradation. *J Manuf Syst*. 2021;59:663-674. doi:10.1016/j.jmsy.2021.04.008
79. Xu P, Li J, Sun C, Yang G, Sun F. Adaptive state-of-charge estimation for lithium-ion batteries by considering capacity degradation. *Electronics*. 2021;10(2):122. doi:10.3390/electronics10020122
80. Agubra V, Fergus J. Lithium ion battery anode aging mechanisms. *Materials (Basel)*. 2013;6(4):1310-1325. doi:10.3390/ma6041310
81. Hall J, Schoen A, Allen P, Liu P, Kirby K. Resistance growth in lithium ion satellite cells. I. Non destructive data analyses. *ECS Meet Abstr*. 2006;MA2005-02(4):242. doi:10.1149/MA2005-02/4/242
82. Schmalstieg J, Kabitz S, Ecker M, Sauer DU. *From accelerated aging tests to a lifetime prediction model: analyzing lithium-ion batteries. Paper presented at: 2013 World Electric Vehicle Symposium and Exhibition (EVS27)*. Barcelona, Spain: IEEE; 2013:1-12. doi:10.1109/EVS.2013.6914753
83. Wikner E, Thiringer T. Extending battery lifetime by avoiding high SOC. *Appl Sci*. 2018;8(10):1825. doi:10.3390/app8101825
84. Li S, He H, Su C, Zhao P. Data driven battery modeling and management method with aging phenomenon considered. *Appl Energy*. 2020;275:115340. doi:10.1016/j.apenergy.2020.115340
85. Ramadass P, Haran B, Gomadam PM, White R, Popov BN. Development of first principles capacity fade model for Li-ion

25784862, 2024, 4, Downloaded from https://onlinelibrary.wiley.com/doi/10.1002/est2.661 by Yildiz Technical University, Wiley Online Library on [13/06/2024]. See the Terms and Conditions (https://onlinelibrary.wiley.com/terms-and-conditions) on Wiley Online Library for rules of use; OA articles are governed by the applicable Creative Commons License

cells. *J Electrochem Soc*. 2004;151(2):A196. doi:10.1149/1.1634273

86. Schimpe M, von Kuepach ME, Naumann M, Hesse HC, Smith K, Jossen A. Comprehensive modeling of temperature-dependent degradation mechanisms in lithium iron phosphate batteries. *J Electrochem Soc*. 2018;165(2):A181-A193. doi:10.1149/2.1181714jes
87. Alhadri M, Zakri W, Esmaeeli R, et al. Analysis of Second-Life of a Lithium-Ion Battery in an Energy Storage System Connected to a Wind Turbine. Paper presented at: IEEE Power Energy Conference at Illinois, PECI. 2019. doi:10.1109/PECI.2019.8698782
88. Alramlawi M, Li P. Design optimization of a residential pv-battery microgrid with a detailed battery lifetime estimation model. *IEEE Trans Ind Appl*. 2020;56(2):2020-2030. doi:10.1109/TIA.2020.2965894
89. Rong P, Pedram M. An analytical model for predicting the remaining battery capacity of lithium-ion batteries. *IEEE Trans Very Large Scale Integr Syst*. 2006;14(5):441-451. doi:10.1109/TVLSI.2006.876094
90. Rezaeimozafar M, Barrett E, Monaghan RFD, Duffy M. Optimal sizing of behind-the-meter battery energy storage systems under optimal battery operation: a case study in Ireland. *J Energy Storage*. 2024;87:111324. doi:10.1016/j.est.2024.111324
91. Liu X, Hu Z, Wang X, Xie M. Capacity degradation assessment of lithium-ion battery considering coupling effects of calendar and cycling aging. *IEEE Trans Autom Sci Eng*. 2024;1-13. doi:10.1109/TASE.2023.3274635
92. Baghdadi I, Briat O, Delétage J-Y, Gyan P, Vinassa J-M. Lithium battery aging model based on Dakin's degradation approach. *J Power Sources*. 2016;325:273-285. doi:10.1016/j.jpowsour.2016.06.036
93. Swierczynski M, Stroe D-I, Stan A-I, Teodorescu R, Kaer SK. Lifetime estimation of the Nanophosphate $LiFePO_4$ battery chemistry used in fully electric vehicles. *IEEE Trans Ind Appl*. 2015;51(4):3453-3461. doi:10.1109/TIA.2015.2405500
94. Javidsharifi M, Pourroshanfekr Arabani H, Kerekes T, Sera D, Spataru S, Guerrero JM. Effect of battery degradation on the probabilistic optimal operation of renewable-based microgrids. *Electricity*. 2022;3(1):53-74. doi:10.3390/electricity3010005
95. Marocco P, Ferrero D, Martelli E, Santarelli M, Lanzini A. An MILP approach for the optimal design of renewable battery-hydrogen energy systems for off-grid insular communities. *Energ Conver Manage*. 2021;245:114564. doi:10.1016/j.enconman.2021.114564
96. Ke X, Lu N, Jin C. Control and size energy storage Systems for Managing Energy Imbalance of variable generation resources. *IEEE Trans Sustain Energy*. 2015;6(1):70-78. doi:10.1109/TSTE.2014.2355829
97. Yan Z, Xu Y, Wang Y, Feng X. *Data-driven economic control of battery energy storage system considering battery degradation. Paper presented at: 9th International Conference on Power and Energy Systems (ICPES)*. Perth, WA: IEEE; 2019:1-5. doi:10.1109/ICPES47639.2019.9105413
98. Steckel T, Kendall A, Ambrose H. Applying levelized cost of storage methodology to utility-scale second-life lithium-ion battery energy storage systems. *Appl Energy*. 2021;300:117309. doi:10.1016/j.apenergy.2021.117309
99. Tang H, Wang S. Life-cycle economic analysis of thermal energy storage, new and second-life batteries in buildings for providing multiple flexibility services in electricity markets. *Energy*. 2023;264:126270. doi:10.1016/j.energy.2022.126270
100. Song Z, Nazir MS, Cui X, Hiskens IA, Hofmann H. Benefit assessment of second-life electric vehicle lithium-ion batteries in distributed power grid applications. *J Energy Storage*. 2022;56:105939. doi:10.1016/j.est.2022.105939
101. Cui J, Tan Q, Liu L, Li J. Environmental benefit assessment of second-life use of electric vehicle lithium-ion batteries in multiple scenarios considering performance degradation and economic value. *Environ Sci Technol*. 2023;57(23):8559-8567. doi:10.1021/acs.est.3c00506
102. Yang J, Beatty M, Strickland D, Abedi-Varnosfaderani M, Warren J. Second-life battery capacity estimation and method comparison. *Energies*. 2023;16(7):3244. doi:10.3390/en16073244
103. Matsushima T. Deterioration estimation of lithium-ion cells in direct current power supply systems and characteristics of 400-ah lithium-ion cells. *J Power Sources*. 2009;189(1):847-854. doi:10.1016/j.jpowsour.2008.08.023
104. He W, Williard N, Osterman M, Pecht M. Prognostics of lithium-ion batteries based on dempster–Shafer theory and the Bayesian Monte Carlo method. *J Power Sources*. 2011;196(23):10314-10321. doi:10.1016/j.jpowsour.2011.08.040
105. Casals LC, Amante García B, Canal C. Second life batteries lifespan: rest of useful life and environmental analysis. *J Environ Manage*. 2019;232:354-363. doi:10.1016/j.jenvman.2018.11.046
106. Ganesh SV, D'Arpino M. Critical comparison of Li-ion aging models for second life battery applications. *Energies*. 2023;16(7):3023. doi:10.3390/en16073023
107. Etxandi-Santolaya M, Canals Casals L, Amante García B, Corchero C. Circular economy-based alternatives beyond second-life applications: maximizing the electric vehicle battery first life. *World Electr Veh J*. 2023;14(3):66. doi:10.3390/wevj14030066
108. Canals Casals L, Etxandi-Santolaya M, Bibiloni-Mulet PA, Corchero C, Trilla L. Electric vehicle battery health expected at end of life in the upcoming years based on UK data. *Batteries*. 2022;8(10):164-180. doi:10.3390/batteries8100164
109. Olmos J, Gandiaga I, Saez-de-Ibarra A, Larrea X, Nieva T, Aizpuru I. Modelling the cycling degradation of Li-ion batteries: chemistry influenced stress factors. *J Energy Storage*. 2021;40:102765. doi:10.1016/j.est.2021.102765
110. D'Arpino M, Cancian M. Lifetime optimization for a grid-friendly DC fast Charge Station with second life batteries. *ASME Lett Dyn Syst Control*. 2021;1(1):1-6. doi:10.1115/1.4046579
111. Nunes TSN, Moura JJP, Prado OG, et al. An online unscented Kalman filter remaining useful life prediction method applied to second-life lithium-ion batteries. *Electr Eng*. 2023;105:3481-3492. doi:10.1007/s00202-023-01910-7
112. Seger PVH, Thivel P-X, Riu D. A second life Li-ion battery ageing model with uncertainties: from cell to pack analysis. *J Power Sources*. 2022;541:231663. doi:10.1016/j.jpowsour.2022.231663
113. Wu W, Lin B, Xie C, Elliott RJR, Radcliffe J. Does energy storage provide a profitable second life for electric vehicle batteries? *Energy Econ*. 2020;92:105010. doi:10.1016/j.eneco.2020.105010
114. Yang F, Wang D, Zhao Y, Tsui K-L, Bae SJ. A study of the relationship between coulombic efficiency and capacity

25784862, 2024, 4, Downloaded from https://onlinelibrary.wiley.com/doi/10.1002/est2.661 by Yildiz Technical University, Wiley Online Library on [13/06/2024]. See the Terms and Conditions (https://onlinelibrary.wiley.com/terms-and-conditions) on Wiley Online Library for rules of use; OA articles are governed by the applicable Creative Commons License

degradation of commercial lithium-ion batteries. *Energy*. 2018;145:486-495. doi:10.1016/j.energy.2017.12.144

115. Cheng M, Ran A, Zheng X, et al. Sustainability evaluation of second-life battery applications in grid-connected PV-battery systems. *J Power Sources*. 2022;550:232132. doi:10.1016/j.jpowsour.2022.232132
116. Cheng M, Zhang X, Ran A, Wei G, Sun H. Optimal dispatch approach for second-life batteries considering degradation with online SoH estimation. *Renew Sustain Energy Rev*. 2023;173:113053. doi:10.1016/j.rser.2022.113053
117. Lam DHC, Wong J, Lim YS, Hau LC. *State of charge, state of health, and degradation estimation for second-life batteries for maximum demand reductions. Paper presented at: 2022 IEEE International Conference on Power and Energy (PECon)*. Malaysia: IEEE; 2022:240-245. doi:10.1109/PECon54459.2022.9988844

How to cite this article: Terkes M, Demirci A, Gokalp E. A comprehensive review of the aging mechanism and degradation costs of fresh and second-life batteries based on analytical and deterministic methods. *Energy Storage*. 2024;6(4):e661. doi:10.1002/est2.661

25784862, 2024, 4, Downloaded from https://onlinelibrary.wiley.com/doi/10.1002/est2.661 by Yildiz Technical University, Wiley Online Library on [13/06/2024]. See the Terms and Conditions (https://onlinelibrary.wiley.com/terms-and-conditions) on Wiley Online Library for rules of use; OA articles are governed by the applicable Creative Commons License